Multi-omics characterization of partial chemical reprogramming reveals evidence of cell rejuvenation

Wayne Mitchell[1], Ludger J.E. Goeminne[1], Alexander Tyshkovskiy[1], Sirui Zhang[1], Julie Y. Chen[1], Joao A. Paulo[2], Kerry A. Pierce[3], Angelina H. Choy[3], Clary B. Clish[3], Steven P. Gygi[2], and Vadim N. Gladyshev[1*]

[1]Division of Genetics, Department of Medicine, Brigham and Women's Hospital, Harvard Medical School, Boston, MA 02115 United States
[2]Department of Cell Biology, Harvard Medical School, Boston, MA 02115 United States
[3]Broad Institute of MIT and Harvard, Cambridge, MA 01241 United States

*Corresponding Author
Dr. Vadim N. Gladyshev
77 Avenue Louis Pasteur
Boston, MA 02115
e-mail: vgladyshev@rics.bwh.harvard.edu

ABSTRACT

Partial reprogramming by cyclic short-term expression of Yamanaka factors holds promise for shifting cells to younger states and consequently delaying the onset of many diseases of aging. However, the delivery of transgenes and potential risk of teratoma formation present challenges for *in vivo* applications. Recent advances include the use of cocktails of compounds to reprogram somatic cells, but the characteristics and mechanisms of partial cellular reprogramming by chemicals remain unclear. Here, we report a multi-omics characterization of partial chemical reprogramming in fibroblasts from young and aged mice. We measured the effects of partial chemical reprogramming on the epigenome, transcriptome, proteome, phosphoproteome, and metabolome. At the transcriptome, proteome, and phosphoproteome levels, we saw widescale changes induced by this treatment, with the most notable signature being an upregulation of mitochondrial oxidative phosphorylation. Furthermore, at the metabolome level, we observed a reduction in the accumulation of aging-related metabolites. Using both transcriptomic and epigenetic clock-based analyses, we show that partial chemical reprogramming reduces the biological age of mouse fibroblasts. We demonstrate that these changes have functional impacts, as evidenced by changes in cellular respiration and mitochondrial membrane potential. Taken together, these results illuminate the potential for chemical reprogramming reagents to rejuvenate aged biological systems and warrant further investigation into adapting these approaches for *in vivo* age reversal.

INTRODUCTION

Cellular aging is accompanied by various features, such as epigenetic changes, upregulation of inflammation, metabolic dysfunction, decreased proteostatic clearance, and increased DNA damage[1-5]. However, while all these hallmarks consistently show changes during aging, there are only limited insights into their potential causative roles. Additionally, many therapies that have targeted single 'hallmarks' of aging have failed to increase lifespan or improve biological functions *in vivo*[6,7]. An alternative way to discover therapies for targeting biological age is to develop tools to quantify it, and then screen interventions for their effect on biological age reduction. Several methods currently exist for quantifying cell aging, such as epigenetic clocks that use mean methylation levels of CpG sites that change during aging[8], transcriptomic clocks that rely on age-associated changes in gene expression[9,10], telomere clocks that rely on age-dependent attrition[11], and various proteomic, metabolomic, and glycomic clocks[12-15]. The development of tools that aim to quantify biological aging have undergone significant improvements over the years. Most notably, second-generation epigenetic clocks trained to predict phenotypic measures and mortality instead of chronological age have been shown to outperform many of these aforementioned clocks in their ability to predict lifespan and healthspan[16].

Using various methods for biological age prediction, several intervention strategies have recently been shown to slow and/or reverse biological aging. These include pharmacological interventions such as rapamycin and metformin[17-20], genetic interventions[21], heterochronic parabiosis[22,23], and partial reprogramming by doxycycline-induced expression of Yamanaka factors[24-26]. A natural rejuvenation process during early development has also been described[27,28]. While partial reprogramming of somatic cells has been shown to lead to improvements in biological function lost during aging[29,30], the effective *in vivo* delivery of the transgenic cassettes and precise control of the expression of Yamanaka factors present challenges. To date, no peer-reviewed studies have demonstrated lifespan increase of wild type animals upon the treatment.

Recently, administration of cocktails of small-molecule compounds have been shown to reprogram somatic cells back to pluripotency[31,32]; moreover, short-term administration of two chemical cocktails (7c and 2c) has demonstrated efficacy at ameliorating several hallmarks of aging in human fibroblasts, while simultaneously preserving cellular identity[33]. Thus, partial reprogramming by short-term administration of chemicals could represent a more feasible, controllable, and adaptable method for inducing rejuvenation *in vivo.* However, the effects of short-term chemical reprogramming on biological age and function are currently unknown, and the mechanisms by which these chemical reprogramming cocktails act are not fully elucidated.

To address this knowledge gap, we have studied the effects of short-term partial cellular reprogramming by chemicals in both young and aged mouse fibroblasts using a multi-tiered approach. In essence, we have systematically evaluated the impact of chemical reprogramming on (i) the epigenome, transcriptome, proteome, phosphoproteome, and metabolome using various omics-based approaches, (ii) biological age with epigenetic and transcriptomic clocks, and (iii) cellular function using gene set enrichment analyses (GSEA) and measurements of cellular respiration. We demonstrate that partial chemical reprogramming induces widespread molecular changes that occur irrespective of the age of the cells. Moreover, we find significant upregulation of mitochondrial OXPHOS complexes in all treatment conditions at the transcriptome and proteome levels. Importantly, mitochondrial OXPHOS is downregulated in aging, and conversely upregulated by many lifespan-increasing interventions. Using both epigenetic and transcriptomic clocks, we show that 7c, but not 2c, reduces biological age in both young and old fibroblasts. Finally, we show that upregulation of mitochondrial OXPHOS by short-term 7c treatment strongly increases spare respiratory capacity and basal mitochondrial transmembrane potential levels. Taken together, these results imply that partial chemical reprogramming by 7c can rejuvenate several aspects of cellular aging, and that regulation of mitochondrial OXPHOS may play an important role in aging and rejuvenation.

MATERIALS AND METHODS

Materials and animals

Young (4-month-old) and old (20-month-old) male C57BL/6 mice were acquired from the National Institute on Aging (NIA) aged rodent colonies (Charles River Laboratories, Wilmington, MA) and were fed standard 5053 chow. HEK293T cells were acquired from ATCC (Manassas, VA) and were verified by PCR to be free of mycoplasma contamination. Cell culture reagents were acquired from ThermoFisher Scientific (Waltham, MA), reagents for isolating DNA and RNA were from Qiagen (Hilden, Germany) and Zymo Research (Irvine, CA), respectively, and general preparatory chemicals and reagents were from Sigma-Aldrich (St. Louis, MO). Chemical reprogramming reagents were obtained from the following suppliers: Sigma-Aldrich (repsox, trans-2-Phenylcyclopropylamine, DZNep), Cayman Chemical Company (TTNPB, CHIR99021), Tocris Bioscience (forskolin), and STEMCELL Technologies (valproic acid). Tetramethylrhodamine, methyl ester perchlorate (TMRM) was obtained from MedChem Express (Monmouth Junction, NJ). Antibodies were obtained from Abcam (Cambridge, United Kingdom). All experiments using mice were performed in accordance with institutional guidelines for the use

of laboratory animals and were approved by the Brigham and Women's Hospital and Harvard Medical School Institutional Animal Care and Use Committees.

Isolation of mouse fibroblasts

Fibroblasts were isolated from the ears and tails of male C57BL/6 mice according to a published procedure[34]. In brief, mice were euthanized by exposure to CO_2 and cervical dislocation, after which ears and 5 cm of tail were sterilized in 70% ethanol for 5 minutes. After air drying, tissues were cut into small, ~3 mm pieces and digested with a mixture of collagenase and pronase for 90 minutes at 37°C with gentle shaking. Following enzymatic digestion, the tissues were ground in 70 µm cell strainers using a 10 ml syringe plunger, and the resulting cell suspension was centrifuged at 500xg for 5 minutes at room temperature. The cell pellet was resuspended in fresh fibroblast culture media (DMEM/F12, 10% FBS, 1X antibiotic-antimycotic, 50 µM β-mercaptoethanol, 1X non-essential amino acids), spun once more at 500xg, resuspended in 10 ml fibroblast culture media, plated in 10 cm tissue culture dishes, and incubated for 3 days at 37°C, 5% CO_2, and 3% O_2. Following 3 days of incubation, media was replaced to get rid of cellular debris, and the cells were then incubated further until reaching ~80% confluency. Upon reaching the desired confluency, ear and tail fibroblasts were trypsinized and frozen at 1 million cells per cryovial in fibroblast freezing media (fibroblast culture media with 50% FBS and 10% DMSO).

Production of lentivirus

HEK293T cells were cultured in high glucose DMEM plus sodium pyruvate, GlutaMAX, 10% FBS, and 1X antibiotic-antimycotic, and were grown to ~70% confluency at 37°C, 5% CO_2. Viral vectors VSVG and gag/pol 8.91, along with either the polycistronic OSKM cassette[35] (Addgene #20328) or the reverse tetracycline transactivator[36] (Addgene #20342), were encapsulated in PureFection nanoparticles (System Biosciences, Palo Alto, CA) and added drop-by-drop to the culturing cells. After 48 and 72 hours, the cell culture media was collected through a 0.45 um filter, spun at 3,000 RPM for 15 minutes at room temperature, and the resulting supernatant was aliquoted and stored at -80°C.

OSKM reprogramming of fibroblasts

Fibroblasts were seeded in 6-well plates at a cell density of 100,000 cells per well in fibroblast culture media and were incubated for 24 hours at 37°C, 5% CO_2, 3% O_2. Fibroblasts were subsequently co-transfected with 1 ml of each lentivirus (OSKM and reverse tetracycline

transactivator), 8 µg/ml polybrene, and 1 ml fresh fibroblast culture media for 3-4 days. Following 3-4 days of transfection, cells were trypsinized and plated on Geltrex® (ThermoFisher, Waltham, MA) coated dishes and incubated for 48 hours. Then, the media was aspirated and replaced with ES media (fibroblast culture media with 20% FBS, 1000 U/ml mouse Leukemia Inhibitory Factor (LIF), and 2 µg/ml doxycycline) and the cells were cultured for 1-2 weeks until colonies appeared (media replaced every 3 days). Colonies were then manually picked, trypsinized, and plated in Geltrex® coated 24-well plates in N2B27 (1:1 mixture of DMEM/F12: 1X N2 supplement, 7.5% BSA, 1X non-essential amino acids, 100 µM β-mercaptoethanol, 1X antibiotic-antimycotic, and Neurobasal: 1X B27 supplement, 7.5% BSA, 1X non-essential amino acids, 1X GlutaMAX, 100 µM β-mercaptoethanol, 1X antibiotic-antimycotic) media, plus 1 µM PD0325901, 3 µM CHIR99021, 0.5 µM Stemolecule™ A83-01, 1000 U/ml LIF, and 2 µg/ml doxycycline. Colonies that survived in this media were deemed to be fully reprogrammed iPSCs and were further propagated into Geltrex® coated 10 cm dishes and cryofrozen in 50% N2B27 media (without inhibitors or doxycycline), 40% FBS, and 10% DMSO at a cell density of 2 million cells per vial.

AP staining

Fibroblasts were seeded at a density of 100,000 cells per well in 6-well plates, and cells were treated with the specified compounds for 4 or 6 days at 37°C, 5% CO_2, 3% O_2 (media and treatments replenished every 3 days). Cells were washed twice with PBS-T, fixed, and stained with the Stemgent AP Staining Kit II according to the manufacturer's protocol (ReproCELL USA, Inc. Beltsville, MD). Cells were then imaged under a brightfield microscope.

Membrane potential staining

Fibroblasts were stained with 250 nM TMRM and 10 µg/ml Hoechst 33342 in fibroblast culture media for 20 minutes at 37°C, 5% CO_2, and 3% O_2. Then, the media was aspirated, and fibroblasts were washed three times with PBS before imaging in the dark on an AXIO Observer.Z1 (Zeiss, Oberkochen, Baden-Württemberg, Germany). As a positive control, cells were pre-treated with 50 µM of carbonyl cyanide m-chlorophenylhydrazone (CCCP) for 15 minutes prior to incubation with TMRM. Images taken from random fields (4-5 images per treatment condition per biological replicate) were background-subtracted in ImageJ[37], and mean fluorescence was normalized to the number of nuclei per field.

Immunocytochemistry

Cells in 24-well plates were rinsed twice with PBS, fixed in 4% paraformaldehyde for 20 minutes at room temperature, and rinsed twice more with PBS. Then, cells were permeabilized with 0.3% Triton X-100 in PBS for 5 minutes, followed by blocking with 3% BSA for 1 hour at room temperature with gentle shaking. After this, cells were incubated with the indicated primary antibody overnight at 4°C, rinsed in the morning with PBS for 2 cycles (10 minutes each), and incubated with fluorophore-conjugated secondary antibody for 1 hour at room temperature in the dark. Cells were then finally stained with 10 µg/ml Hoechst 333342 for 10 minutes, rinsed 3 times with PBS, and imaged on an AXIO Observer.Z1 inverted fluorescence microscope (Zeiss, Oberkochen, Baden-Württemberg, Germany).

DNA methylation

DNA was isolated from cells using the DNeasy Blood and Tissue kit according to the manufacturer's instructions (Qiagen, Hilden, Germany). Concentration of DNA samples was measured using the Qubit dsDNA BR kit (Invitrogen, Waltham, MA). DNAmAge (using various epigenetic clocks) was assessed using DNA methylation data obtained on the Horvath mammal 320k array[38] through the Epigenetic Clock Development Foundation (Torrance, CA). Raw methylation array data was normalized using SeSAMe[39]. Probes were filtered and removed based on the following criteria: missing values or a p-value of detection > 0.01 for any samples, not mappable to the mouse *mm10* reference genome and technical controls for the array.

All DNA methylation analysis was performed in the R/Bioconductor environment. Probe-wise differential methylation analysis was performed using limma using M-values, since this method has been shown to be more statistically robust for identifying significantly differentially methylated probes (DMPs) when compared to using beta values[40]. Significantly DMPs were identified using a cutoff threshold where |log2FC(M-value)| > 1 and Benjamini-Hochberg false discovery rate < 0.05. Enrichment of the significantly DMPs for specific chromatin states was assessed using a universal chromatin state annotation of the mouse genome spanning 26 cell and tissue types[41]. Briefly, we calculated odds ratios of observing significantly up- or down-regulated DMPs in each chromatin state and performed a one-sided hypergeometric test (*phyper)* to test for significance of enrichment or depletion. We report signed $\log_{10}$ p-values, adjusted using the Benjamini-Hochberg method, of either enrichment (OR > 1, sign = +1) or depletion (OR <= 1, sign = -1) depending on the odds ratio.

RNA-seq

Fibroblasts were seeded in 6-well plates at a cell density of 100,000 cells per well in fibroblast culture media and were incubated for 6 days at 37°C, 5% CO_2, 3% O_2 with their respective chemical treatments (media replaced once after 3 days). On the 6th day, media was aspirated, and the cells were washed twice with PBS. Then, the cells were directly lysed with 700 µl of Trizol, diluted 1:1 with 200 proof ethanol, and total RNA was isolated using a direct-zol mini prep kit (Zymo Research, Irvine, CA). RNA concentration was measured by Qubit using the RNA HS assay kit (ThermoFisher, Waltham, MA). Libraries were prepared with TruSeq Stranded mRNA LT Sample Prep Kit according to TruSeq Stranded mRNA Sample Preparation Guide, Part # 15031047 Rev. E. Libraries were quantified using the Bioanalyzer (Agilent) and sequenced with Illumina NovaSeq6000 S4 (2×150bp) (reads trimmed to 2×100bp) to get 20M read depth coverage per sample. The BCL (binary base calls) files were converted into FASTQ using the Illumina package bcl2fastq. Fastq files were mapped to the mm10 (GRCm38.p6) mouse genome, and gene counts were obtained with STAR v2.7.2b[42]. Statistical analyses for gene expression were performed with custom models from *DEseq2*[43] 3.13 and *edgeR*[44] 3.34.1 in R. We filtered out genes with low number of reads, keeping only the genes with at least 5 reads in at least 20% of the samples, which resulted in 16,728 detected genes according to Entrez annotation. Filtered data was then passed to Relative Log Expression (RLE) normalization. Differential expression of genes perturbed by compounds was analyzed using *edgeR*. Obtained p-values were adjusted for multiple comparison with the Benjamini-Hochberg method.

Association with gene expression signatures of aging and OSKM reprogramming

Association of gene expression log-fold changes in aged fibroblasts and induced by chemical reprogramming cocktails with established transcriptomic signatures of aging and OSKM reprogramming was examined with GSEA-based method as described previously[45]. The utilized signatures of aging included tissue-specific liver, kidney, and brain signatures as well as multi-tissue signatures of the mouse, rat, and human[46]. Signatures of OSKM reprogramming included genes differentially expressed during cellular reprogramming of mouse fibroblasts (Mouse), and shared transcriptomic changes during OSKM-induced reprogramming of mouse and human fibroblasts (Mouse and Human)[26]. For every signature, top 500 statistically significant genes (adjusted p-value < 0.05) with the highest absolute logFC were used as gene sets for GSEA-based association analysis. Pairwise Spearman correlation for gene expression and protein abundance changes induced by chemical reprogramming as well as transcriptomic signatures of aging and OSKM reprogramming was calculated based on the union of top 650 genes with the lowest p-value for each pair of signatures.

For the identification of enriched functions affected in aged fibroblasts or by 2c or 7c treatment, we performed functional GSEA[47] on a pre-ranked list of genes or proteins based on $\log_{10}$(p-value) corrected by the sign of regulation, calculated as:

$$-log(pv) \times sgn(lfc),$$

where *pv* and *lfc* are p-value and logFC of a certain gene, respectively, obtained from edgeR output, and *sgn* is the signum function (equal to 1, -1 and 0 if value is positive, negative or equal to 0, respectively). Gene ontology: biological process (GObp), HALLMARK, KEGG and REACTOME ontologies from the Molecular Signature Database (MSigDB) were used as gene sets for GSEA. The GSEA algorithm was performed separately for each cocktail and age group via the *fgsea* package in R with 5000 permutations. p-values were adjusted with the Benjamini-Hochberg method. A false discovery rate cutoff of 0.1 was used to select statistically significant functions. A similar analysis was performed for gene expression signatures of aging and OSKM reprogramming.

Transcriptomic clock analyses

To assess the transcriptomic age (tAge) of fibroblasts treated with chemical reprogramming reagents, we applied multi-tissue mouse transcriptomic clocks based on the identified signatures of aging[46]. Filtered RNAseq count data was passed to log transformation and scaling. The missing values corresponding to clock genes not detected in the data were imputed with the precalculated average values. Pairwise differences between average tAges of fibroblasts subjected to chemical reprogramming and corresponding controls were assessed using independent t-tests.

Measurement of splicing damage

The RNA sequencing reads were aligned to the mouse genome (mm10) using STAR with the parameters "--chimSegmentMin 2 --outFilterMismatchNmax 3 --alignEndsType EndToEnd", and Percent Spliced-In (Psi) values were calculated using rMATS[48]. To identify the alternative splicing changes after compounds treatment, we compared the alternative splicing events between 7c treatment and paired control sample and selected the events with significant differences (with the cutoff of $|\Delta Psi\ avg| > 0.1$, and FDR < 0.05). To quantify the overall damage caused by splicing changes, we also counted the proportion of the events that may disrupt protein function. In detail, we predicted the functional consequence for each alternative splicing event and counted the following three categories for each sample: (1) Introduction of a premature stop

codon; (2) Production of frameshifted proteins; and (3) Loss of a peptide in a protein domain region.

Sample processing for quantitative TMT-proteomic analysis

For TMT18-plex proteomics, a slightly modified form of published procedures was utilized[49,50]. In brief, fibroblasts were seeded at a density of 1 million cells per 10 cm dish and were treated with the specified compounds for 6 days (media replaced once after 3 days) at 37°C, 5% CO_2, 3% O_2. Following completion of the incubation period, cells were rinsed twice with cold PBS and scraped and collected in 0.4 ml of modified RIPA buffer (50 mM KPO_4 (pH 7.5), 150 mM NaCl, 1% Triton X-100, 0.5% deoxycholate, 1% SDS, and 1X protease and phosphatase inhibitors). Samples were then vortexed for 30 seconds, placed on ice for 10 minutes, and pelleted at 21,000 x g for 10 minutes (4°C). The supernatants were transferred to fresh microfuge tubes, and protein concentration was measured by BCA assay (ThermoFisher, Waltham, MA). Then, 200 µg of each protein sample was reduced with 5 mM TCEP, alkylated with 10 mM iodoacetamide, quenched with 10 mM DTT, and chloroform-methanol precipitated. The protein pellets were briefly dried in a speed-vac and resuspended in 100 µl of 200 mM EPPS, pH 8.5. Protein samples were digested with 1:100 Lys-C:protein overnight at room temperature, followed by 1:100 trypsin:protein for 6 hours at 37°C.

The samples were then labeled with tandem mass tag (TMTpro) reagents[49]. Acetonitrile was added to a final volume of 30% prior to adding the TMTpro labeling reagent. For protein level analysis, ~50 µg of peptides were labeled with 100 µg of TMT. For phosphopeptide analysis, we estimated the phosphopeptide enrichment to be ~1.5:100 and so ~30 µg of peptides were labeled with 60 µg of TMT. Labeling occurred at room temperature for 1h. ~2 µg of peptide from each sample was pooled, desalted and analyzed by mass spectrometry to check labeling efficiency.

TMT labeling efficiency was determined using the “label-check” sample, which is a quality control step prior to the final pooling of TMT-labeled samples. Here, we combined a small amount (1-3 µl or ~2µg) of each sample and analyzed it by mass spectrometry to confirm that peptide digestion was successful, if the degree of labeling was sufficient, and if the labeled samples contained approximately equal amount of peptides. During database searching, the TMTpro label was considered a variable modification at the N-terminus and at lysine residues. We then determined the labeling efficiency for the N-terminus and the lysine residues by dividing labeled N-terminal peptides by total peptides and then labeled lysine-containing peptides by the total lysine-containing peptides. The labeling efficiency should be greater than 95% before proceeding with the analysis. Once labeling efficiency was verified (here, >97%), hydroxylamine was added

at a final concentration of ~0.3% and incubated for 15 min. at room temperature. The remaining samples were pooled at a 1:1 ratio across all channels.

To enrich phosphopeptides, the pooled sample was desalted over a 200 mg SepPak column and phosphopeptides were enriched with the Pierce High-Select Fe-NTA Phosphopeptide enrichment kit following manufacturer's instructions. The eluate was desalted via StageTip[51] and is ready for MS analysis. The washes and the unbound fraction of this enrichment were desalted and used for proteome-level analysis.

For proteome-level analysis, the pooled sample was fractionated using basic-pH reversed-phase (BPRP) Liquid Chromatography using an Agilent 1200 pump with an Agilent 300Extend C18 column (2.1 mm ID, 3.5 µm particles, and 250 mm in length). The flow rate over the column was 0.25 mL/min and we used a 50-min linear gradient with 5% to 35% acetonitrile in 10 mM ammonium bicarbonate pH 8. Ninety-six fractions were collected and concatenated into 24 superfractions prior to desalting[52]. These 24 superfractions were sub-divided into two groups, each consisting of 12 non-adjacent superfractions. These superfractions were subsequently acidified with 1% formic acid and vacuum centrifuged to near dryness. Each superfraction was desalted via StageTip[51]. Once dried by vacuum centrifugation, the sample was reconstituted using 5% formic acid and 5% acetonitrile prior to acquisition of LC-MS/MS data.

Mass spectrometry data collection and processing

Mass spectrometric data were collected on an Orbitrap Fusion Lumos mass spectrometer, both which are coupled to a Proxeon NanoLC-1200 UHPLC and a FAIMSpro interface[53]. The 100 µm capillary column was packed with 35 cm of Accucore 150 resin (2.6 µm, 150 Å; ThermoFisher Scientific).

Data for the protein superfractions were acquired on an Orbitrap Lumos with a CV set of -40/-60/-80V over a 90 min gradient using Realtime search (RTS)-MS3. The scan sequence began with an MS1 spectrum (Orbitrap analysis, resolution 60,000, 350−1350 Th, automatic gain control (AGC) target 5 $x10^5$, maximum injection time 100 ms). MS2 analysis consisted of collision-induced dissociation (CID), quadrupole ion trap analysis, automatic gain control (AGC) 2 $x10^4$, NCE (normalized collision energy) 35, q-value 0.25, maximum injection time 120 ms), and isolation window at 0.5 Th. RTS was enabled and quantitative SPS-MS3 scans (resolution of 50,000; AGC target $2.5x10^5$; max injection time of 250 ms) with a real-time false discovery rate filter implementing a modified linear discriminant analysis. For FAIMS, the dispersion voltage (DV) was set at 5000V, the compensation voltages (CVs) used were -40V, -60V, and -80V, and the TopSpeed parameter was set at 1 sec.

For phosphopeptide profiling, data were acquired using two injections on an Orbitrap Lumos one with a CV set of -40/-60/-80V and a second injection with a CV set of -30/-40/-50V, both over a 150 min gradient. A 1sec TopSpeed cycle was used for each CV. The scan sequence began with an Orbitrap MS1 spectrum with the following parameters: resolution: 60,000, scan range: 350-1350 Th, automatic gain control (AGC): 100%, and maximum injection time: 118 ms. MS2 analysis consisted of higher-energy collisional dissociation (HCD) with the following parameters: resolution: 50,000, AGC: 300%, normalized collision energy (NCE): 36%, maximum injection time: 250 ms, and isolation window: 0.7 Th, and. In addition, unassigned, singly, and > 5+ charged species were excluded from MS2 analysis and dynamic exclusion was set to 60 s.

Once the spectra were converted to mzXML using MSconvert[54], database searching could be performed. Database searching included all mouse entries from UniProt (downloaded March 2022), which was concatenated with a version of the database in which the order of the amino acid residues of each protein was reversed. Database searches used a 50-ppm precursor ion tolerance and a product ion tolerance of 0.03 Da. We have traditionally used the 50ppm mass tolerance for our Sequest, and now Comet, database searches. These wide mass tolerance windows were chosen to maximize sensitivity in conjunction with Comet searches and linear discriminant analysis[55,56]. For static modifications, lysine residues and peptide N-termini were modified with +304.207 Da due to the TMTpro labels. Meanwhile, all cysteine residues were modified with iodoacetamide (carbamidomethylation) that results in a +57.021 Da increase in mass. Also, methionine oxidation (+15.995 Da) was set as a variable modification. Likewise, deamidation (+0.984 Da) at glutamine and asparagine residues and phosphorylation (+79.966 Da) at serine, threonine, and tyrosine residues were also set as variable modifications for phosphopeptide enrichment. The false discovery rate (FDR) was set at 1% at the peptide level with filtering by linear discriminant analysis[57]. The protein lists were assembled further to a final protein-level FDR of 1%. The intensities of reporter ions were corrected for the isotopic impurities of the different TMT reagents[58]. For each protein, the peptide-summed signal-to-noise (S/N) measurements were summed and normalized to account for equal protein loading by equating the sum of the signal for all proteins in each channel.

For further processing, normalized Uniprot ID-level intensities were summed and $\log_2$ transformed to obtain unique intensities at the level of gene symbol identifiers. Differential abundance analysis was performed with msqrob2[59,60] (https://github.com/statOmics/msqrob2), where we included treatment (control, 2c, or 7c), age group (4 months, or 20 months), and the treatment:age group interaction as covariates. For the phosphoproteomics data, the normalized relative phosphopeptide intensities were $\log_2$ transformed. Differential abundance analysis at the

level of these normalized relative log_2 phosphopeptides intensities was again performed in msqrob2[59,60] with the same covariates as for the proteomics analysis. We performed GSEA to obtain protein-level enrichments from the phosphopeptides. To obtain pathway enrichments for both the proteomics and phosphoproteomics data, we ran the GSEA algorithm with the HALLMARK, KEGG, and REACTOME ontologies from the Molecular Signature Database[47] (MSigDB). For kinase substrate enrichment analysis, we performed GSEA using the mouse kinase substrate dataset from PhosphoSitePlus[61] (last updated on April 19th, 2023).

Seahorse assays

Fibroblasts treated with vehicle, 2c, or 7c for 6 days as described above were seeded on 24-well cell culture plates overnight at 37°C, 5% CO_2, 3% O_2 at a cell density of 50,000 cells per well. The following morning, the cells were aspirated and the media was replaced with 500 µl of XF DMEM medium (pH 7.4) supplemented with 1 mM sodium pyruvate, 2 mM glutamine, and 10 mM glucose. Cells were incubated for 1 hour at 37°C in a non-CO_2 incubator prior to assessment of oxygen consumption rate (OCR) and extracellular acidification rate (ECAR) on a XeF24 Extracellular Flux Analyzer (Agilent Technologies, Santa Clara, CA) using a standard Mito Stress protocol[62]. Immediately following the end of the run, cells were stained with LCS1 nuclear green and cells were counted on a SpectraMax i3 plate reader (Molecular Devices, San Jose, CA). OCR and ECAR measurements were then normalized to cell count per well.

Preparation of metabolite samples

Cells were incubated with their respective treatments for 6 days, and then the cells were rinsed with ice-cold 0.9% saline solution. After rinsing, cells were scrapped into 1 ml of 0.9% saline solution, spun at 2,000 x g for 2 minutes (4°C), aspirated, and flash frozen in liquid nitrogen. To extract metabolites, the cells were thawed, lysed in 400 µl of ice-cold methanol, 200 µl of ice-cold chloroform was added, and then another 200 µl of chloroform and 300 µl of ultrapure water was added and the resulting mixture was vortexed for 30 seconds. Following incubation on ice for 10 minutes, the samples were spun at 4,000 rpm for 10 minutes (4°C), and the upper polar phases (600 µl) were transferred to fresh microfuge tubes and stored at -80°C until ready for analysis by mass spectrometry. For normalization of metabolite peak area values, 400 µl of methanol was added to the leftover samples (consisting of nonpolar phases and precipitated protein), and the samples were vortexed and spun at 20,000xg for 5 minutes (4°C). Protein pellets were then aspirated, air-dried for 30 minutes, and resuspended in 500 µl of modified RIPA buffer.

Protein concentrations were measured by BCA assay (ThermoFisher, Waltham, MA), and metabolite peak areas were divided by the total amount (µg) of protein in each sample.

Metabolite profiling

Hydrophobic interaction liquid chromatography (HILIC) positive ionization profiling was carried out on a Shimadzu Nexera X2 U-HPLC (Shimadzu Corp.; Marlborough, MA) coupled to an Exactive Plus hybrid quadrupole Orbitrap mass spectrometer (Thermo Fisher Scientific; Waltham, MA) according to a published procedure[63]. Protein was precipitated from 10 µl of sample by addition of nine volumes of 74.9:24.9:0.2 v/v/v acetonitrile/methanol/formic acid containing internal standards (valine-d8, Sigma-Aldrich; St. Louis, MO; and phenylalanine-d8, Cambridge Isotope Laboratories; Andover, MA). Precipitated material was cleared by centrifugation and the supernatant was injected directly onto a 150 x 2 mm 3 µm Atlantis HILIC column (Waters; Milford, MA). Elution was as follows: (1) 5% mobile phase A (10 mM ammonium formate and 0.1% formic acid in water), 0.5 min, 250 µl/min; (2) linear gradient to 40% mobile phase B (acetonitrile with 0.1% formic acid), 10 min, 250 µl/min. MS analysis was with electrospray ionization (ESI) in positive ion mode with the following parameters: full scan analysis over 70–800 m/z at 70,000 resolution and 3 Hz data acquisition rate; sheath gas 40; sweep gas 2; spray voltage 3.5 kV; capillary temperature 350°C; S-lens RF 40; heater temperature 300°C; microscans 1; automatic gain control target 1e6; and maximum ion time 250 ms.

HILIC negative ionization profiling[63] was carried out on an Shimadzu Nexera X2 U-HPLC (Shimadzu Corp.; Marlborough, MA) coupled to a Q Exactive Plus hybrid quadrupole orbitrapmass spectrometer (Thermo Fisher Scientific; Waltham, MA). Protein was precipitated from 30 µl of sample by addition of four volumes of 80% methanol containing internal standards (inosine-15N4, thymine-d4 and glycocholate-d4; Cambridge Isotope Laboratories; Andover, MA). Precipitated material was cleared by centrifugation and the supernatant was injected directly onto a 150 x 2.0 mm Luna NH2 column (Phenomenex; Torrance, CA). Elution was as follows: (1) 10% mobile phase A (20 mM ammonium acetate and 20 mM ammonium hydroxide in water) and 90% mobile phase B (10 mM ammonium hydroxide in 75:25 v/v acetonitrile/methanol), 400 µl/min; (2) linear gradient to 100% mobile phase A, 10 min, 400 µl/min. MS analysis was with electrospray ionization (ESI) in the negative ion mode with the following parameters: full scan analysis over m/z 70–750 at 70,000 resolution and 3 Hz data acquisition rate; sheath gas 55; sweep gas 10; spray voltage −3.0 kV; capillary temperature 350°C; S-lens RF 50; heater temperature 325 °C; microscans 1; automatic gain control target 1e6; and maximum ion time 250 ms.

Raw data was processed using TraceFinder (Thermo Fisher Scientific; Waltham, MA) and Progenesis QI (Nonlinear Dynamics; Newcastle upon Tyne, UK) for Q Exactive (Plus) experiments or MultiQuant (SCIEX; Framingham, MA) for 5500 QTRAP experiments. Metabolite identities were confirmed using authentic reference standards or reference samples.

Annexin V assay

Cells were seeded in 6-well plates at a density of 200,000 cells per well, and treated for either 1, 3, or 6 days with 7c or vehicle (media and treatments replaced after 3 days). Following their specified treatment times, cells were trypsinized, neutralized, and spun at 500xg for 5 minutes at room temperature. Following aspiration, cells were resuspended in 100 µl of Annexin V binding buffer (10 mM HEPES, 2.5 mM $CaCl_2$, 140 mM NaCl) and stained at room temperature with 1 µg/ml DAPI and 5 µl of Annexin V FITC (Tonbo Biosciences, San Diego, CA) for 15 minutes in the dark. Following this incubation period, 400 µl of binding buffer was added to each solution of cells, the cells were filtered through mesh cell strainers, and cells were immediately analyzed by flow cytometry on a Cytek DxP11 (Cytek Biosciences, Fremont, CA). For each sample, 100,000 events were recorded, and cells were gated based on fluorescence signals of unlabeled cells and single-labeled controls in FlowJo (Ashland, OR).

Prkaca colocalization

Fibroblasts were seeded at a density of 40,000 cells per well in #1.5 chambered coverglass pre-coated with 0.2% gelatin. Cells were then incubated overnight prior to fixation and permeabilization with 4% paraformaldehyde and ice-cold methanol, respectively. Fixed cells were blocked with 3% BSA and stained with Alexa Fluor 488 goat anti-mouse for mouse anti-Prkaca, and Alexa Fluor 568 goat anti-rabbit for rabbit anti-Tom20 (Bio-Techne, Minneapolis, MN), and 10 µg/ml DAPI. Imaging was performed on a Zeiss LSM980 Airyscan2 Point Scanning Confocal using a 63X/1.4 oil objective. Image analysis was performed in ImageJ[37]. Training and access to this instrument was provided by the Microscopy Resources on the North Quad (MicRoN) core at Harvard Medical School.

Prkaca RNAi and measurement of mitochondrial membrane potential

For RNAi, cells were seeded at a density of 100,000 cells per well in 6-well plates and incubated overnight at 37°C, 5% CO_2, 3% O_2. Then, cells were transfected with either 15 nM Silencer® pre-designed siRNA targeting Prkaca or a nontargeting siRNA (negative control) using Lipofectamine™ RNAiMAX Transfection Reagent prepared in Opti-MEM™ reduced serum

media. Cells were cultured for 6 days total, with media and treatments (siRNA:lipofectamine complexes and drug cocktails) replaced after 3 days. After 6 days, membrane potential staining and imaging was performed as previously described.

To verify successful knockdown of Prkaca, cells were trypsinized and pelleted after 3 days of RNAi. Cell pellets were then aspirated, resuspended in SDS-PAGE sample buffer, and resolved on 4-20% TGX gels. Blots were performed using monoclonal antibodies against Prkaca (Santa Cruz Biotechnology Inc., Dallas, TX) and GAPDH (ThermoFisher, Waltham, MA). Percent knockdown of Prkaca was assessed relative to GAPDH abundance using ImageJ[37].

Statistical analyses and rigor

Each independent biological replicate for this study consists of fibroblasts isolated from a single mouse treated with each cocktail. A technical replicate represents fibroblasts from the same mouse with the same treatment but measured independently. All measurements in this study consist of at least 3 independent biological replicates. The type I error rate was controlled at the 5% level, either by student's t-test, or by controlling the family-wise error rate at 5% by one-way ANOVA and Tukey's post-hoc analysis, where appropriate. For large omics experiments, the false discovery rate was controlled with the Benjamini-Hochberg procedure at the 5% level, unless stated otherwise.

RESULTS

Partial chemical reprogramming increases pluripotency and mitochondrial OXPHOS activity

For this study, we freshly isolated tail and ear fibroblasts from young (4-month-old, or '4 month') and old (20-month-old, or '20 month') male C57BL/6 mice (**Figure 1A**). We only used fibroblasts that had been passaged ≤ 3 times to ensure that they maintain a physiologically relevant aged phenotype in cell culture. Indeed, previous studies have shown that the epigenetic age of fibroblasts increases rapidly once they are cultured *in vitro*[64]. For our study, we used two cocktails: 7c (repsox, trans-2-phenylcyclopropylamine, DZNep, TTNPB, CHIR99021, forskolin, and valproic acid), which can reprogram somatic cells to pluripotency[31,32]; and 2c (repsox, trans-2-phenylcyclopropylamine), a subset of 7c that does not negatively affect cell proliferation[33]. First, we initiated treatment for 4 days prior to assessing their effects on pluripotency by staining for alkaline phosphatase (AP) activity[65] (**Figure 1B**). While neither 7c nor 2c treatment appeared to affect fibroblast morphology, 2c treatment dramatically increased the number of cells positive for AP activity in both young and old fibroblasts, an indication of increased pluripotency. In contrast, 7c treatment had no effect on AP activity.

Next, we assessed the effect of partial chemical reprogramming (6 days treatment with 2c or 7c) on resting mitochondrial membrane potential and mitochondrial mass using TMRM fluorescence. Previous studies have established a decline of mitochondrial membrane potential with age[66], that caloric restriction (a well-characterized longevity intervention) acts by increasing mitochondrial membrane potential[67], and that artificially increasing the mitochondrial membrane potential of *C. elegans* extends their lifespan[68]. Thus, characterizing the effect of partial chemical reprogramming on basal mitochondrial membrane potential may be a reporter of its efficacy in rejuvenating cells. We observed a strong increase in normalized TMRM fluorescence upon 2c and 7c treatment, and this effect was mirrored across young and old fibroblasts (**Figure 1C**). As a control, we pre-treated fibroblasts with the mitochondrial uncoupler CCCP and observed the expected decrease in TMRM signal relative to fibroblasts treated with vehicle. Thus, we concluded that partial chemical reprogramming strongly impacts mitochondrial bioenergetics during basal conditions.

Given these results, we further wanted to establish the effect of partial chemical reprogramming on mitochondrial function. To this end, we performed Seahorse experiments on fibroblasts treated with 7c and 2c (**Figure 1D**) using the Mito Stress Test protocol[62]. In order to account for the effects of these cocktails on cell proliferation, we stained and counted the cells with LCS1 immediately after the run finished, and normalized the oxygen consumption rates (OCR) to OCR per 10,000 cells. From the raw traces, we observed similar responses between young and old fibroblasts. While 2c and 7c treatment only had minor effects on basal oxygen consumption rates, 7c dramatically increased both proton leak (mitochondrial oxygen consumption with inhibited ATP synthase minus non-mitochondrial respiration) and spare respiratory capacity (uncoupled minus basal respiration). Furthermore, these results were corroborated by the observed increase in mitochondrial mass and magnitude of the mitochondrial membrane potential in response to 7c treatment. Taken together, we concluded that partial chemical reprogramming, particularly with 7c, strongly increases the activity and/or abundance of mitochondrial oxidative phosphorylation (OXPHOS) complexes.

Partial chemical reprogramming ameliorates aging-related changes in gene expression and reduces splicing damage

To investigate the effects of partial chemical reprogramming on gene expression, and in particular on the expression of mitochondrial OXPHOS genes, we performed bulk RNA-seq (**Figure 2**) on young and old fibroblasts treated for 6 days with 7c and 2c. By principal component analysis (PCA) (**Figure 2A**), we observed that fibroblasts treated with 7c are strongly separated

from control and 2c treatment by principal component 1, whereas control and 2c treated fibroblasts are separated by principal component 2. Moreover, when we assessed the association of gene expression changes caused by fibroblast age (**Figure 2 – figure supplement 1A**, left panel) with previously established signatures of OSKM reprogramming and aging[26,46], we saw positive association with multiple tissue-specific (kidney, liver) and multi-tissue (mouse and rat) signatures of aging, and negative association with the mouse signature of OSKM-induced iPSCs. Thus, at the level of gene expression, the aged phenotype of the 20-month-old fibroblasts was preserved *in vitro*. However, the number of differentially expressed genes with 2c and 7c treatment (**Figure 2B**) far exceeded the number of differentially expressed genes modified by age (**Figure 2 – figure supplement 1A**, right panel). Accordingly, changes induced by 2c or 7c were highly correlated across tested age groups (Spearman correlation coefficient > 0.8) (**Figure 2 – figure supplement 1B**). We first quantified the effect of partial chemical reprogramming on the expression of pluripotency markers[69-71] and the transcription factors *Klf4* and *c-Myc* (*Myc*) (**Figure 2C**). *Bend4*, *Esrrb*, and *Klf4* were all upregulated following partial chemical reprogramming, and this occurred irrespective of the age of the fibroblasts. However, 2c treatment also upregulated expression of *Myc* and *Sox2*, whereas 7c treatment did not. Furthermore, 7c somewhat paradoxically reduced expression of *Nanog* and *Myc*. Thus, 2c treatment appeared to have a more pronounced pro-pluripotency effect, which was supported by the increase in AP-positive cells following partial chemical reprogramming. Moreover, 7c had differing effects on pluripotency despite 2c being a subset of this cocktail. Thus, short-term partial chemical reprogramming with 7c appeared to show a different mechanism than normal OSKM cellular reprogramming[72], whereas 2c in contrast appeared to share more similarities with OSKM reprogramming.

Since the accumulation of numerous types of cellular damage is thought to be causal to the aging process[73], we next wanted to see if partial chemical reprogramming could reverse the accumulation of damaged splice variants. To this end, we characterized the alternative splicing events as a function of age (**Figure 2 – figure supplement 2A**) and quantified the proportion of splicing events that may affect protein function (**Figure 2D**). For 7c-treated fibroblasts, we observed a significant lowering of splicing-related protein damage. Furthermore, we noticed a marginally significant elevation of splicing-related damage with age, whereas the relative proportions of alternative splicing events remained unchanged. To further characterize the effect of 7c treatment on alternative splicing, we assessed the distribution of ΔPsi values of differentially spliced (|ΔPsi| > 0.1 and p-value < 0.05) genes for old (**Figure 2 – figure supplement 2B**) and young (**Figure 2 – figure supplement 2C**) fibroblasts, separated by the type of alternative splicing. While the number of differentially spliced events with positive and negative ΔPsi values

for exon skipping was roughly equivalent, there was an excess of events with negative ΔPsi values for intron retention across both age groups. Thus, 7c treatment appeared to reduce splicing damage by decreasing the number of retained introns with functional consequences.

To further characterize gene expression changes induced by 2c and 7c, we also assessed their association with the signatures of OSKM reprogramming and aging[26,46]. Consistent with previous results, we observed significant positive association between signatures of OSKM reprogramming, both in mice and humans, and gene expression changes induced by 2c treatment in fibroblasts from both age groups (**Figure 2E**). In contrast, transcriptomic profiles of fibroblasts treated with 7c didn't exhibit consistent positive association with markers of OSKM-induced iPSCs. Besides, gene expression changes induced by both 2c and 7c were negatively associated with signatures of aging corresponding to different tissues and mammalian species, suggesting that partial chemical reprogramming may indeed counteract molecular features of aging.

Partial chemical reprogramming increases the abundance of mitochondrial OXPHOS complexes

To elucidate the effects of partial chemical reprogramming on cellular function, we performed multi-plexed proteomics (**Figure 3**) using isobaric tandem mass tags[49]. PCA based on the normalized protein abundances (**Figure 3A**) showed strong separation of 7c (principal component 1) and 2c (principal component 2) treatments from control. This effect was further visualized by heatmap (**Figure 3B**), which demonstrated that 7c treatment had a much more profound effect than 2c. Protein abundances and gene expression changes induced by 2c or 7c treatments were well correlated with each other (**Figure 3C, Figure 3 – figure supplement 1A**), with Spearman correlation coefficients > 0.7. Furthermore, genes differentially expressed at both the mRNA and proteins levels (**Figure 3 – figure supplement 1A**) following partial chemical reprogramming were generally conserved across the age groups and treatments (**Figure 3 – figure supplement 1B**). Finally, by Spearman correlation analyses of proteomics samples (**Figure 3 – figure supplement 1C**), we observed clustering by both treatment type and age group. Thus, we concluded that 7c treatment had a profound effect on the cellular proteome, and that our proteomics and RNA-seq analyses were in general agreement with each other.

To gain insight into the functional processes associated with the observed anti-aging effect of partial chemical reprogramming, we performed gene set enrichment analysis (GSEA) of the gene expression and protein abundance changes produced by 2c and 7c, along with signatures of aging and OSKM reprogramming (**Figure 3D**). In aging signatures, we observed a significant upregulation of pathways involved in inflammation, apoptosis, and p53 signaling, accompanied by a downregulation of genes related to energy metabolism and DNA repair. Furthermore, for

aging in the fibroblast system used in this study, we also observed an upregulation of apoptosis, inflammation, and interferon signaling, thus further validating these fibroblasts isolated from aged mice as an appropriate system to study aging *in vitro*. When we examined all pathways affected by age at the protein level (**Figure 2 – figure supplement 1C**, left panel), we further identified several other upregulated pathways classically associated with aging, including Mtorc1 and Kras signaling, and hypoxia.

In contrast, OSKM reprogramming in both human and mouse models counteracted most of these age-related changes. Interestingly, treatment with 2c and 7c also produced multiple anti-aging effects, particularly at the protein level, including upregulation of OXPHOS, TCA cycle, fatty acid metabolism, and mitochondrial translation, and downregulation of interferon signaling. Surprisingly, genes and proteins associated with p53 pathway were upregulated by both cocktails. Partial chemical reprogramming also affected the abundance of proteins involved in cellular differentiation and extracellular matrix organization, resembling the effect of OSKM-induced iPSCs. Many of the pathways upregulated by fibroblast age at the protein level were counteracted by treatment with 7c and 2c, with Mtorc1 signaling being a notable exception in that it appeared to be even more strongly activated by 7c treatment in old fibroblasts (**Figure 2 – figure supplement 1C**, center and right panels). Finally, 7c treatment resulted in a significantly lower concentration of proteins associated with the PI3K/Akt signaling, suggesting that this intervention may induce pro-longevity mechanisms. Thus, partial chemical reprogramming ameliorated multiple molecular features of aging at the level of individual genes, proteins and cellular pathways, and reproduced several effects of OSKM reprogramming.

Since the anti-aging effects of partial chemical reprogramming on the proteome were more pronounced than their effects on the transcriptome, we then used GSEA on the proteomics data to find pathways affected by 7c and 2c treatments (**Figure 3 – figure supplement 2A**). Many mitochondrial-related processes were upregulated by partial chemical reprogramming, whereas only functions related to cell proliferation and cell cycle were downregulated. Notably, all mitochondrial OXPHOS complexes (I-V, **Figure 3E**) were upregulated for both treatments in both age groups. Proteins essential for mRNA splicing were downregulated by both age and partial chemical reprogramming, although 7c downregulated more splicing-involved proteins than 2c (**Figure 3 – figure supplement 2B**). Additionally, proteins essential for RNA methylation were upregulated in both 2c and 7c-treated fibroblasts, with more pronounced effects observed with 7c. This observation could be relevant for the reduced splicing damage after 7c treatment, as RNA methylation is known to affect mRNA splicing[74]. Finally, we studied the effects of partial chemical reprogramming on other proteins relevant for aging, such as chaperones[75], collagens[76],

and proteins implicated in the mitochondrial unfolded protein response[77] (UPR^{mt}, **Figure 3 – figure supplement 2B**). Whereas UPR^{mt} was upregulated by both 7c and 2c, chaperones were significantly upregulated only by 7c treatment, and collagen proteins were down in 7c and up in 2c. Taken together, these results suggested that partial chemical reprogramming strongly upregulated mitochondrial function, with 7c treatment having a more profound effect.

Finally, we examined Spearman correlation of changes in both mRNA and protein abundance induced by 2c and 7c with gene expression signatures of OSKM reprogramming and aging (**Figure 4**). Consistent with our previous findings, we observed a significant positive association between OSKM reprogramming features and the effects of 2c, both at the gene expression and protein abundance levels. Furthermore, the transcriptomic and proteomic changes induced by 2c and 7c were negatively correlated with multiple signatures of mammalian aging. Therefore, partial chemical reprogramming demonstrated the ability to reduce molecular signatures of aging at both the protein and mRNA levels.

Partial chemical reprogramming phosphorylates mitochondrial proteins and activates Prkaca signaling

In addition to using multi-plexed proteomics to quantitatively ascertain overall effects on protein expression, we also evaluated the effects of partial chemical reprogramming on protein phosphorylation and kinase signaling by using TMT-based phosphoproteomics (**Figure 5**). First, we performed GSEA on the normalized relative phosphopeptide intensities. Across all treatments and age groups, we observed decreased phosphorylation of proteins involved in cell migration and proliferation, and conversely increased phosphorylation of proteins essential to fatty acid metabolism, signaling and transport of ions, and muscle development and contraction (particularly in 2c-treated fibroblasts) (**Figure 5 – figure supplement 1A**). More generally, shared across 2c and 7c treatments was an upregulation in the phosphorylation of mitochondrial proteins (**Figure 5A**). In addition, for 2c-treated fibroblasts, proteins involved in lipolysis and constructing muscle were also increasingly phosphorylated. Although 7c treatment reduced splicing damage (**Figure 2E**), we observed no statistically significant changes in the phosphorylation of proteins required for mRNA splicing. Overall, we determined that 2c and 7c treatment share a common mechanism in upregulating OXPHOS activity by phosphorylating mitochondrial proteins, with 7c having a stronger effect relative to 2c. We also observed that 2c treatment activated additional pathways (lipolysis and muscle contraction) compared to 7c.

To dive deeper into the mechanisms of partial chemical reprogramming, we analyzed kinase signaling pathways affected by 2c and 7c treatments (**Figure 5B**). For all treatments and

age-groups, only Prkaca signaling was significantly (FDR < 0.05) and consistently upregulated. Notably, Prkaca, the catalytic alpha subunit of the cAMP-activated protein kinase A, is crucial for regulating glucose metabolism, and upon activation, for increasing lipolysis and energy expenditure in white adipose tissue[78]. Thus, it is interesting that this kinase was activated by 7c treatment when no statistically significant effect on lipolysis was observed with this treatment. In contrast, in young fibroblasts, Akt1 and Mapk1 signaling was significantly upregulated and downregulated, respectively upon 2c treatment. Both pathways were also strongly affected by 2c treatment in old fibroblasts but did not reach statistical significance (FDR > 0.05). Mapk1 and Akt1 have opposing effects on regulating the expression of structural constituents of muscle[79]; thus, this observed influence is entirely consistent with upregulation of proteins involved in muscle contraction by 2c treatment. Therefore, we concluded that 2c and 7c share similar mechanisms of partial chemical reprogramming via activation of Prkaca signaling and mitochondrial phosphorylation. However, activation of Prkaca by 7c treatment had different downstream effects than by 2c treatment.

Prkaca is dispensable for mediating increase in mitochondrial membrane potential following partial chemical reprogramming with 7c

Next, we wanted to verify if Prkaca signaling activated by partial chemical reprogramming was necessary to mediate its effects on the upregulation of mitochondrial OXPHOS. To this end, we knocked down Prkaca in old fibroblasts using RNA interference and assessed its impact on mitochondrial membrane potential during 7c partial chemical reprogramming (**Figure 5C**, left panel). While Prkaca was successfully knocked down to approximately 25% of its basal level as analyzed by Western blot (**Figure 5 – figure supplement 1B**), TMRM fluorescence of 7c-treated *Prkaca* knockdown fibroblasts was not statistically different from either 7c-treated control knockdown fibroblast treatments (treated with 7c only, or 7c and a non-targeted siRNA). Thus, we concluded that Prkaca signaling is either not necessary for mediating the increase in mitochondrial membrane potential caused by 7c treatment, or the amount of Prkaca remaining after knockdown is sufficient to mediate the required level of signaling. Despite this, we did observe a change in cellular distribution of Prkaca following 7c treatment (**Figure 5C**, right panel) by confocal microscopy. Instead of translocating to mitochondria, we observed that Prkaca appeared to localize to the nucleus more strongly during partial chemical reprogramming with 7c in old fibroblasts. Therefore, Prkaca could have a functional role in moderating some of the transcriptional responses to partial chemical reprogramming.

Finally, we checked the effect of partial chemical reprogramming with 7c on apoptosis in old fibroblasts using Annexin V staining and flow cytometry (**Figure 5 – figure supplement 1C**). During the course of partial chemical reprogramming, we observed a steady increase in the percentage of apoptotic cells (DAPI negative, Annexin V FITC positive) that reached a maximum of approximately 20% on day 6. This percentage of apoptotic cells is similar to what has been reported with OSK/OSKM reprogramming[80]. Thus, these data suggest that the majority of cells successfully undergo partial chemical reprogramming by 7c treatment.

Partial chemical reprogramming reverses the accumulation of aging-related metabolites

As the levels of endogenous cellular metabolites can have both activating and inhibitory effects on various signaling pathways, we performed an untargeted mass spectrometry-based analysis of metabolites following partial chemical reprogramming (**Figure 6**). We analyzed the abundance of polar metabolites (polar fraction taken from chloroform-methanol extraction of cell pellets) by hydrophobic interaction liquid chromatography (HILIC)[81,82]. Again, to account for the effects of chemical reprogramming cocktails on cell proliferation rates, we measured the protein concentration in each cell pellet by BCA assay and normalized the peak area of each metabolite by the amount (µg) of protein per sample. By PCA (**Figure 6 – figure supplement 1A**), we saw a clear separation of 7c treatment from control and 2c by principal component 1, whereas only young fibroblasts treated with 2c were separated from control by principal component 2. Furthermore, when we looked at just the metabolite samples from untreated fibroblasts, we observed a clear separation by fibroblast age (**Figure 6 – figure supplement 1B**). All samples were separated based on their respective treatments by hierarchical clustering (**Figure 6A**), and of 203 different metabolites detected, 109 were significantly altered by the different treatment groups (**Figure 6B**).

We visualized the metabolites altered by partial chemical reprogramming by both heatmap (**Figure 6C**) and volcano plots (**Figure 6 – figure supplement 1C**). These analyses revealed that the levels of many metabolites, including guanidoacetic acid, creatine, and several nucleotides, were affected by fibroblast age. Moreover, 7c treatment had a much more pronounced effect on the metabolome than 2c, which agreed with both the previous functional and multi-omics data. Since only some of the metabolites affected by fibroblast age were subsequently counteracted by 7c treatment, these data suggested that rather than targeting specific aging-related changes, 7c treatment appeared to divert cells to a different metabolic state. Analysis of the top 50 significantly altered metabolites (**Figure 6D**) revealed a cluster of 6 metabolites strongly upregulated by 7c treatment (guanidoacetic acid, S-adenosylhomocysteine (SAH), tyramine, tributylamine,

trimethylamine N-oxide, and atenolol). Interestingly, SAH is known as an inhibitor of DNA methyltransferases, both by product build-up and by competitive inhibition[83,84]. Thus, the increased abundance of SAH upon 7c treatment could stem from changes in epigenetic regulation through the activity of DNA methyltransferases, especially since protein levels of Mat2a were decreased by 7c treatment (**Figure 6E**, top). Guanidoacetic acid, on the other hand, is the biosynthetic precursor of creatine and accepts a donor methyl group from S-adenosyl methionine[85] (SAM). Therefore, the effects of 7c treatment on guanidoacetic acid and SAH levels were intertwined. Conversely, many metabolites were strongly downregulated by 7c treatment, including 3',5' cyclic AMP (an activator of protein kinase A[78]), xanthine (an inhibitor of phosphodiesterases that increase cyclic AMP levels[86]), and various other purines, nucleosides, and nucleotides (hypoxanthine, inosine, pseudouridine, uridine, uracil, adenosine, and guanosine). In agreement with this observation, proteins involved in xanthine metabolism (**Figure 6E**, bottom) were upregulated by partial chemical reprogramming with 7c. Moreover, several purine degradation metabolites have been shown to be positively associated with aging[87], suggesting that 7c treatment may reverse the accumulation of aging-related metabolites.

In the case of 2c treatment, two upregulated and related metabolites stood out: serotonin, and its biosynthetic precursor 5-hydroxy-tryptophan (5-HTP), which is decarboxylated to form serotonin[88]. Besides being an important neurotransmitter, serotonin and its precursor 5-HTP are formed downstream from tryptophan by tryptophan hydroxylase and 5-HTP decarboxylase.[88] While the abundance of tryptophan itself was not altered by partial reprogramming, the abundance of niacinamide, which is also synthesized from tryptophan[89], was slightly reduced following 2c treatment. Lastly, for 2c, two byproducts of lysine metabolism (Glu-Lys and aminoadipic acid) were downregulated, whereas lysine levels were not statistically altered. Since lysine is crucial for the cross-linking of collagen fibrils[90], and since 2c strongly upregulated the expression of collagen proteins (**Figure 3E**), 2c treatment could be downregulating lysine catabolism. Therefore, we observed strong effects of partial reprogramming on the cellular metabolome, and these effects were generally consistent with the analyses of protein and gene expression. Additionally, partial chemical reprogramming with 7c appeared to reduce the levels of several purine derivatives, which could be important for reducing aging-related accumulation of damaging metabolites.

Partial chemical reprogramming rejuvenates both young and aged cells

To assess the rejuvenation potential of partial chemical reprogramming, we analyzed the effect of 7c and 2c treatment on fibroblast age (**Figure 7**) using mouse multi-tissue transcriptomic

clocks (**Figure 7A**). As tools to measure age, transcriptomic clocks have successfully reported the effects of interventions known to affect lifespan and rate of biological aging, and appear to be sensitive to transient changes in gene expression that may occur upon short-term treatment with drugs[9,10] and OSKM reprogramming[26]. Application of transcriptomic clocks developed in our lab to the bulk RNA-seq dataset (presented in **Figure 2**) revealed a statistically significant decrease of both chronological and biological age with short-term 7c treatment in young and old fibroblasts; however, only the chronological clock reported a significant, but less prominent, reduction of transcriptomic age following 2c treatment. Additionally, the chronological transcriptomic clock revealed that the 20-month-old untreated primary fibroblasts were transcriptionally older than 4-month-old fibroblasts, which suggested that the fibroblast system used in this study demonstrated age-related changes in gene expression shared across multiple mouse organs. However, when the lifespan-adjusted biological clock was applied, no statistical significance was observed. Thus, we determined that the 20-month-old fibroblasts used in our study did not exhibit substantial changes in gene expression associated with decreased healthspan, while 7c had substantial effects on both general and mortality-associated age-related transcriptomic changes.

We also measured DNA methylation (DNAm) by microarrays following partial chemical reprogramming, and analyzed the results using relevant epigenetic clocks[91] (**Figure 7B**). As a positive control, we measured the epigenetic ages (DNAmAge) of young and old fibroblasts reprogrammed by OSKM expression (**Figure 7 – figure supplement 1**). We found a consistent lowering of DNAmAge in response to 7c treatment, whereas the effect of 2c treatment was weaker and more variable, depending on the clock used. As expected, fibroblasts isolated from old mice were epigenetically older than fibroblasts taken from young mice, which further confirmed that the fibroblasts maintained their aged phenotype in cell culture. Finally, fully-reprogrammed fibroblasts (iPSCs) demonstrated an epigenetic age of approximately 0, which was consistent with previous reports[8]. Therefore, we concluded that partial chemical reprogramming, particularly by 7c treatment, can rejuvenate both young and aged cells.

When we further analyzed the effects of fibroblast age on the epigenome, we observed a significant number of CpG sites that became differentially methylated with age (**Figure 7 – figure supplement 2A**). While these aging-related differences did not impact mean DNAm levels (**Figure 7 – figure supplement 2B**), we did observe an enrichment of hypomethylated CpG sites for active enhancer regions in 20-month-old fibroblasts (**Figure 7 – figure supplement 2C**). When we compared these results with the effects of partial chemical reprogramming, we observed by PCA that the samples were much more strongly separated by treatment condition rather than fibroblast age (**Figure 7 – figure supplement 3A**). OSKM- and 7c-reprogrammed cells were

clearly separated from control samples, whereas 2c-reprogrammed cells were not. This was made further evident by the fact that 7c treatment caused a greater number of CpG sites to become significantly differentially methylated than 2c treatment (**Figure 7 – figure supplement 3B**). Furthermore, rather than targeting specific CpG sites that changed with fibroblast age, 7c treatment induced global hypomethylation (**Figure 7 – figure supplement 3C**) that consequently caused the reduction in cell epigenetic age. Moreover, hypomethylated CpG sites after 7c-treatment were enriched for transcription and exon regions and conversely, depleted at heterochromatin and promote regions (**Figure 7 – figure supplement 3D**). This signature was shared in both young and old fibroblasts, suggesting that 7c-treatment appeared to push cells to a distinct epigenetic landscape independent of their initial state.

DISCUSSION

The goal of our study was to characterize the effects of partial chemical reprogramming of cells at the level of the epigenome, transcriptome, proteome and phosphoproteome, and metabolome. To do this, we used low-passage fibroblasts isolated from young (4-month-old) and old (20-month-old) C57BL/6 male mice and treated the fibroblasts with two chemical reprogramming cocktails (2c and 7c). We then analyzed the effects of partial chemical reprogramming and its relationship to aging using a suite of omics-based approaches. Finally, we combined these multi-omics assays with measures of biological age (by using aging clocks) and cellular function (by utilizing respirometry and fluorescence microscopy to determine the effects of partial chemical reprogramming on mitochondrial bioenergetics). Together, these studies evaluated the potential for partial chemical reprogramming to ameliorate aging features, and uncovered its associated mechanisms for further optimization and development of treatments that could slow and/or reverse aging *in vivo*.

Based on measurements of biological age using epigenetic and transcriptomic clocks, we concluded that partial chemical reprogramming with 7c was able to rejuvenate fibroblasts taken from both young and old mice. Additionally, from measures of mRNA, protein, and phosphoprotein abundances, we determined that partial chemical reprogramming causes wide-scale changes to fibroblast gene expression that are larger in magnitude than the changes that occur due to aging. Based on GSEA analyses of these multi-omics data, we uncovered that the most prominent mechanistic signature of partial chemical reprogramming is the upregulation of mitochondrial oxidative phosphorylation, which further manifested as a functional increase in spare respiratory capacity and increased mitochondrial transmembrane potential. Moreover, this increase in OXPHOS activity was accompanied by a slight increase in apoptosis during the course of

reprogramming, suggesting that partial chemical reprogramming might remove cells with dysfunctional mitochondria. Finally, we showed that partial chemical reprogramming can reverse molecular damage positively associated with aging, including the accumulation of aging-related metabolites and mis-spliced mRNA.

The downregulation of mitochondrial OXPHOS and translation is a known signature of aging[45,46]; furthermore, several recent studies have highlighted that augmenting the mitochondrial transmembrane potential can increase longevity[67,68]. In this light, we suggest that partial chemical reprogramming of fibroblasts induces rejuvenation, at least in part, by upregulating mitochondrial OXPHOS. Importantly, this differs significantly from OSKM reprogramming, which shows a strong glycolytic shift in response to the induction of OSKM expression[92]. Furthermore, our results are consistent with the activation of different transcription factors by partial chemical reprogramming with 7c, which showed negligible expression of the Yamanaka factors, increased expression of two pluripotency markers (*Esrrb* and *Bend4*), and decreased expression of *Nanog*.

The results of several recent studies have illustrated the changes in mitochondrial ultrastructure that occur during aging[93-95], which may result from several interdependent mechanisms such as disrupted OPA1-,Drp1-, and MICOS-mediated fission and fusion dynamics[96-100], decreased cardiolipin content[101], destabilized ATP synthase dimers[102], and uncontrolled opening of the mitochondrial permeability transition pore[103,104]. Importantly, mitochondrial ultrastructure determines bioenergetic function and thus, detrimental changes to mitochondrial ultrastructure (such as loss of tight cristae junctions and cristae curvature) can lead to bioenergetic declines during aging[105,106]. These declines include increased proton leak and reactive oxygen species production[105-107], decreased respiratory supercomplex assembly and associated spare respiratory capacity[106,108], and impaired proteostasis[109,110]. Thus, the activation of factors that reinforce proper mitochondrial ultrastructure could reverse many aging-related elements of mitochondrial dysfunction.

It should be emphasized that across most assays, the effects of partial chemical reprogramming were similar in both young and old fibroblasts. In simplest terms, this could be because the changes observed due to fibroblast aging (i.e. in terms of the number of differentially expressed genes, proteins, and metabolites) were approximately an order of magnitude lower than those observed with partial chemical reprogramming. An alternative, non-mutually exclusive explanation is that partial chemical reprogramming, particularly with 7c, pushes cells to a different metabolic state that makes them biologically younger (i.e. at the transcriptional and epigenome levels) as a byproduct. For example, with the untreated fibroblasts, we observed an increased epigenetic age in the 20-month-old fibroblasts without a change in mean DNAm. In contrast, with

7c treatment, we saw decreased epigenetic age in both young and old fibroblasts that occurred due to induced global hypomethylation. Thus, we believe that 7c-mediated partial chemical reprogramming may activate a unique set of transcription factors that produce an epigenetically-distinct cellular state, irrespective of the initial state of the epigenome and in addition to the known de-methylating effects of DZNep.

In conclusion, we have shown that partial chemical reprogramming is able to reverse many signs of aging in a mouse fibroblast model. We thus posit that partial reprogramming by chemicals may represent a viable alternative to the cyclically-induced, ectopic expression of Yamanaka factors for rejuvenating aged cells. There are several limitations of OSK/OSKM partial reprogramming, including low efficiency[111,112], oncogenic risk[112], and potential toxicity due to varying cell types being reprogrammed at different rates[113]. In this study, we have shown that partial chemical reprogramming with 7c features a distinct mechanism from OSK/OSKM partial reprogramming; thus, partial chemical reprogramming could potentially circumvent these risks because it activates different transcriptional programs to reduce cellular biological age. Furthermore, as druggable small-molecule compounds, dosages and delivery agents can be precisely tailored to modify their pharmacokinetics and tissue distributions, and to minimize their cellular toxicity and potential off-target effects. Further testing however, particularly in animal models of aging, is needed to fully elucidate the effectiveness of partial chemical reprogramming *in vivo*, and to establish what advantages, if any, it may have over OSK/OSKM partial reprogramming. In addition, it is important to note that this study was performed using only one cell type isolated from inbred male mice; different cell types experience varying changes during aging[114], and the effects of aging and lifespan-extending interventions are generally sex-dimorphic[115]. Thus, extensive validation in multiple cell types and in genetically-diverse male and female mice is necessary to determine if partial chemical reprogramming can ameliorate several relevant dimensions of mammalian aging. In addition, a more thorough characterization of the effect of partial chemical reprogramming on mitochondrial dynamics and function, such as OXPHOS supercomplex assembly, cristae ultrastructure, and protein import, could shed greater light on the importance of various mitochondrial processes in the aging process. Finally, elucidating the molecular targets of chemical reprogramming compounds, whether they may be transcription factors, regulators of the epigenome, and/or various kinases and cellular receptors, could further contribute to our understanding of aging and how to best reverse it.

ACKNOWLEDGEMENTS

The authors would like to thank Dr. William Oldham for assistance with Seahorse measurements, Bobby Brooke for coordinating measurements of DNAm by microarray, Jesse Poganik for assistance with analysis of metabolomics data, and members of the Gladyshev lab for helpful discussions.

The project described was supported by the National Institute of Biomedical Imaging and Bioengineering, National Institutes of Health through grant number T32 EB016652 to W.M, by NIA grants to V.N.G., and by NIH/NIGMS grant R01 GM132129 (to J.A.P.) and GM67945 (to S.P.G.).

CONTRIBUTIONS

W.M designed the study, conducted the experiments, and wrote the original draft. L.J.E.G analyzed proteomics and phosphoproteomics data and performed GSEA. A.T performed GSEA, and transcriptomic clock and signature analyses. S.Z performed splicing analyses of RNA-seq data. J.Y.C analyzed DNAm microarray data. J.A.P performed TMT labeling and acquired mass spectrometry data. K.A.P and A.H.C analyzed the metabolomics samples. C.B.C supervised acquisition of metabolomics data and provided funding. S.P.G supervised acquisition of proteomics data and provided funding. V.N.G designed and supervised the study and provided funding. All authors contributed to the revision of the manuscript.

FIGURE LEGENDS

Figure 1: Functional effects of partial chemical reprogramming

A. Overview of the study. Tail and ear fibroblasts were isolated from young (4-month-old) and old (20-month-old) male C57BL/6 mice, and cryo-stocks were prepared once reaching ~80-90% confluency (passage number P1). All fibroblasts used in this study were ≤ P3. These cells were subjected to partial chemical reprogramming followed by indicated analyses. *B. AP staining.* Young and old fibroblasts were treated with 2c, 7c, or DMSO for 4 days, followed by visualization of cells positive for alkaline phosphatase activity with the StemAb™ Alkaline Phosphatase Staining Kit II (4X objective). Scale bars: 126.2 µm (100 pixels). *C. TMRM staining.* Following treatment for 6 days with 2c, 7c, or DMSO, fibroblasts were stained with 250 nM TMRM and 10 µg/ml Hoechst 33342 for 20 minutes at 37°C, 5% CO_2, and 3% O_2. TMRM fluorescence intensity was normalized to the number of nuclei per field and quantified across 4-5 images from random fields for each independent biological replicate (n = 3). For CCCP treatment, cells were treated with 50 µM CCCP in DMSO for 15 minutes prior to TMRM staining. Error bars represent means ± standard deviations, and data were quantified based on percent change from control-treated

fibroblasts. Scale bars: 31.1 µm (100 pixels). Statistical significance was determined by one-way ANOVA and Tukey's post-hoc analysis. *p < 0.05, **p < 0.01, ***p < 0.001. *D. Effects on oxygen consumption.* Top: representative raw traces of oxygen consumption of cells subjected to the Mito Stress Test protocol (basal, followed by 1 µM oligomycin a, 5 µM FCCP, and 1 µM rotenone / antimycin a) following 6 days of partial chemical reprogramming. Error bars represent means ± standard deviations from 3 technical replicates per treatment. Bottom: quantified oxygen consumption rates across 4 independent biological replicates (n = 4, error bars represent means ± standard deviations). Statistical significance was determined by one-way ANOVA and Tukey's post-hoc analysis. *p < 0.05, **p < 0.01, ***p < 0.001.

Figure 2: Effect of partial chemical reprogramming on gene expression

A. PCA of bulk RNA-seq samples. Fibroblasts were treated with 2c, 7c, or control for 6 days followed by RNA-seq analyses. *B. Differentially expressed genes.* Differentially expressed genes were determined using *edgeR* and considered statistically significant at a Benjamini-Hochberg false discovery rate (FDR) cut-off < 0.05. *C. Expression of pluripotency markers.* Effect of partial chemical reprogramming on the normalized expression of pluripotency markers and *Klf4* and *c-Myc* (*Myc*). Statistical inference was performed with *edgeR*. *p.adjusted < 0.05, **p.adjusted < 0.01, ***p.adjusted < 0.001. *D) Splicing damage.* Splicing damage was determined by the proportion of alternative-splicing events that may disrupt protein function. Statistical significance was determined by one-way ANOVA and Tukey's post-hoc analysis. ^p < 0.1, *p < 0.05. *E. Association of gene expression changes induced by chemical reprogramming with signatures of aging and OSKM reprogramming.* Signatures of aging are labelled in red, whereas signatures of OSKM reprogramming are labelled in cyan. NES: normalized enrichment score. Statistical inference was done with the fgsea R package. *FDR < 0.05, **FDR < 0.01, ***FDR < 0.001.

Figure 3: Effect of partial chemical reprogramming on protein expression

A. PCA of log_2 normalized protein abundances. Fibroblasts were treated for 6 days with 2c, 7c, or control followed by mass spectrometry-based proteomic analyses. *B. Global effects of partial chemical reprogramming on the proteome.* Scaled heatmap of normalized protein abundances with clustering. *C. Comparisons between effects on protein and gene expression.* Log_2 fold changes of protein (vertical axis) versus mRNA (horizontal axis) for 20-month-old fibroblasts treated with 7c. Spearman correlation coefficient is shown in bold. Labeled are the genes that are most strongly differentially expressed after 7c treatment (adjusted p-value < 0.05) at both the mRNA and protein levels (shown in green). Also depicted are genes significantly changing only

at the protein level (shown in cyan), or at the mRNA level (shown in red). Spearman correlation coefficients between protein and mRNA levels were > 0.7 for all treatment conditions (refer to **Figure 3 – figure supplement 1**). *D. Functional GSEA.* Pathways enriched by gene expression changes induced by partial chemical reprogramming (blue: 7c, green: 2c) and aging in primary fibroblasts (red) from the current study, as well as by established signatures of OSKM reprogramming (cyan) and aging (red). ^Benjamini-Hochberg FDR < 0.1, *FDR < 0.05, **FDR < 0.01, ***FDR < 0.001. *E. Effect of partial chemical reprogramming on the expression of protein complexes associated with aging.* Protein abundances of mitochondrial OXPHOS complexes, chaperones, collagens, and the spliceosome are all affected by partial chemical reprogramming. Each datapoint represents the abundance of an individual protein. Significance was assessed with a linear regression model that included effects for gene, treatment, age group, and a treatment:age group interaction. p-values within each panel were corrected for multiple testing with the default Dunnett correction ("single-step") method in the *multcomp* R package[116]. 'adjusted p-value < 0.1, *adjusted p-value < 0.05, **adjusted p-value < 0.01, ***adjusted p-value < 0.001, n.s. adjusted p-value ≥ 0.1.

Figure 4: Correlation of gene and protein expression changes with signatures of aging and OSKM reprogramming

Spearman correlation of gene expression and protein abundance changes induced by partial chemical reprogramming (blue: 7c, green: 2c) with the signatures of OSKM reprogramming (cyan) and aging (red). Correlation coefficients ρ were calculated by the Spearman method based on the union of top 650 genes with the lowest p-value for each pair of signatures. Statistically significant pairwise correlations with Spearman ρ > 0.1 are labelled with asterisks. ***Benjamini-Hochberg FDR < 0.001.

Figure 5: Effect of partial chemical reprogramming on the phosphoproteome

A. Targeted GSEA analysis of phosphorylation targets for four selected gene ontologies following partial chemical reprogramming. Bar lengths depict normalized enrichment scores. **Benjamini-Hochberg FDR < 0.01, ***FDR < 0.001. *B. Kinase signaling pathways.* z-values for a kinase enrichment analysis are shown for the effects of partial reprogramming with 2c (horizontal axis) vs. 7c (vertical axis) in young (top) and old (bottom) fibroblasts. Signaling pathways significantly affected (Benjamini-Hochberg FDR < 0.05) by both 7c and 2c treatment (Prkaca) are colored in red, and signaling pathways affected only by 2c in young fibroblasts (Makp1 and Akt1) are colored in green (highlighted in bold for old fibroblasts). Horizontal and vertical red lines indicate the 0.05

Benjamini-Hochberg FDR significance threshold cut-offs for the comparisons 2c vs. control and 7c vs. control, respectively. *C. Role of Prkaca in partial chemical reprogramming.* Left: knockdown of Prkaca during 7c partial chemical reprogramming in 20-month-old fibroblasts and effects on mitochondrial membrane potential, as assessed by TMRM fluorescence (n = 3 independent biological replicates). p-values were determined by one-way ANOVA and Tukey's post-hoc analysis. ns $p \geq 0.1$, ***$p < 0.001$. Right: staining of 20-month-old fibroblasts for cellular localization of Tom20 (red) and Prkaca (green) during 7c partial chemical reprogramming. Representative images are shown, and data was collected for n = 3 independent biological replicates. Scale bars: 20 µm.

Figure 6: Effect of partial chemical reprogramming on the metabolome

A. Hierarchical clustering of polar metabolite samples. Fibroblasts were treated for 6 days with 2c, 7c, or control followed by cell scraping and collection in cold 0.9% saline solution (n = 3 independent biological replicates). Polar metabolites were isolated from the frozen cell pellets by chloroform-methanol extraction, and the upper polar phase was analyzed by hydrophobic interaction liquid chromatography (HILIC) coupled to a quadrupole mass spectrometer in both positive and negative ionization modes[81,82]. All subsequent analyses were performed using MetaboAnalyst 5.0[117]. *B. Metabolites affected by partial chemical reprogramming.* A total of 203 metabolites were identified by HILIC-positive and -negative methods, combined. Metabolite peak areas were normalized to the amount (µg) of protein in each cell pellet (determined by BCA assay) and log-transformed. In total, abundances of 109 metabolites were significantly altered by partial chemical reprogramming (Benjamini-Hochberg FDR < 0.05, colored in red). *C. Global effects of partial chemical reprogramming on the metabolome.* Scaled heatmap of normalized, log-transformed metabolite abundances. *D. Abundances of top 50 metabolites significantly altered by partial chemical reprogramming with 2c or 7c.* Scaled heatmap with labeled metabolites. *E. Expression of metabolite-related proteins.* Expression of proteins related to s-adenosylhomocysteine biosynthesis (top) and xanthine metabolism (bottom) following partial chemical reprogramming with 2c and 7c vs. control in young and old cells. 'Benjamini-Hochberg FDR < 0.1, *FDR < 0.05, **FDR < 0.01, ***FDR < 0.001.

Figure 7: Effect of partial chemical reprogramming on biological age

A. Effect of partial chemical reprogramming on transcriptomic age (tAge). tAge was assessed by using mouse multi-tissue transcriptomic clocks to analyze the bulk RNA-seq data presented in Figure 2 (n = 4 independent biological replicates). p-values were determined by one-way ANOVA

and Tukey's post-hoc analysis. ns $p \geq 0.1$, ^$p < 0.1$, *$p < 0.05$, **$p < 0.01$. *B. Effect of partial chemical reprogramming on epigenetic age (DNAmAge).* Levels of mean DNA methylation (DNAm) was assessed by DNAm microarray on the Horvath mammal 320k chip (n = 5 independent biological replicates). p-values were determined by one-way ANOVA and Tukey's post-hoc analysis. *$p < 0.05$, **$p < 0.01$, ***$p < 0.001$.

Figure 2 – figure supplement 1: Effect of partial chemical reprogramming on aging-related changes in fibroblast gene and protein expression

A. Effect of fibroblast age on gene expression changes. Left panel: association of aging-related changes in fibroblast gene expression with signatures of aging and OSKM reprogramming. Signatures of aging are labelled in red, whereas signatures of OSKM reprogramming are labelled in cyan. NES: normalized enrichment score. Statistical significance was determined using GSEA as implemented in the fgsea R package. *FDR < 0.05, **FDR < 0.01, ***FDR < 0.001. Right panel: Volcano plot of age-related differentially expressed genes (genes with FDR < 0.05 colored in red, differential expression analysis performed using *edgeR*). *B. Correlation between gene expression changes induced by chemical reprogramming in young and old fibroblasts.* Spearman correlation coefficients are shown in bold. Labeled are the genes that are most strongly differentially expressed after 2c and 7c treatment (Benjamini-Hochberg FDR < 0.05) in young and old fibroblasts (shown in green). Also depicted are genes significantly changing only in old fibroblasts (shown in cyan), or only in young fibroblasts (shown in red). *C. GSEA of aging-related changes in protein expression.* Shown here are comparisons between old and young untreated fibroblasts (left), old 2c-treated and old untreated fibroblasts (center), and old 7c-treated and old untreated fibroblasts (right). 'Benjamini-Hochberg FDR < 0.1, *FDR < 0.05, **FDR < 0.01, ***FDR < 0.001.

Figure 2 – figure supplement 2: Characterization of alternative splicing events

A. Observed alternative splicing events. Observed alternative splicing events in control samples (n = 4 independent biological replicates) grouped by different types of alternative splicing (A3SS = alternative 3' splice site, A5SS = alternative 5' splice site, IR = intron retention, ES = exon skipping) and age. *B. Distribution of alternative splicing changes in old fibroblasts after 7c treatment.* Each datapoint represents one splicing event that was differentially spliced ($|\Delta Psi| > 0.1$ and Benjamini-Hochberg FDR < 0.05) following 7c treatment. *C. Distribution of alternative splicing changes in young fibroblasts after 7c treatment.* Each datapoint represents one splicing event that was differentially spliced ($|\Delta Psi| > 0.1$ and Benjamini-Hochberg FDR < 0.05) following 7c treatment.

Figure 3 – figure supplement 1: Additional correlation analyses

A. Comparisons between protein differential abundance and differential gene expression. Shown here for all treatment conditions (top: 2c vs. control, bottom: 7c vs. control. Left panels: young fibroblasts, right panels: old fibroblasts). Spearman correlation coefficients are shown in bold. *B. Correlations between protein and mRNA levels.* Heatmap of Spearman correlation coefficients across all treatment conditions calculated based on the union of top 1000 genes with the lowest p-value for each pair of signatures (blue: 7c, green: 2c). *C. Correlation between log_2 normalized abundances of the proteomics samples.* Heatmap of Spearman correlation coefficients.

Figure 3 – figure supplement 2: GSEA of protein abundances

A. GSEA (GObp, HALLMARK, KEGG, and REACTOME) most significantly altered by partial chemical reprogramming. Shown are the top 25 most significant ontologies in each comparison (2c and 7c vs. controls, in young and old fibroblasts). 'Benjamini-Hochberg FDR < 0.1, *FDR < 0.05, **FDR < 0.01, ***FDR < 0.001. *B. Protein abundances of processes affected by partial chemical reprogramming.* Log_2 fold changes of proteins involved in alternative mRNA splicing (left), mitochondrial unfolded protein response (UPR^{mt}, center), and RNA methylation (right). 'Benjamini-Hochberg FDR < 0.1, *FDR < 0.05, **FDR < 0.01, ***FDR < 0.001.

Figure 5 – figure supplement 1: Effect of partial chemical reprogramming on cellular signaling

A. GSEA of phosphopeptide abundances. GSEA of phosphorylated pathways significantly altered by partial chemical reprogramming. We show all ontologies with Benjamini-Hochberg FDR < 0.05 in at least one comparison (2c and 7c vs. controls, in young and old fibroblasts). 'Benjamini-Hochberg FDR < 0.1, *FDR < 0.05, **FDR < 0.01. *B. Knockdown of Prkaca and effects on mitochondrial membrane potential.* Upper panels: Western blot showing knockdown of Prkaca in 20-month-old fibroblasts relative to GAPDH levels using RNA interference (n = 3). NC: negative control (non-targeting siRNA). p-value was determined by a two-tailed t-test. ***p < 0.001. Lower panels: representative images of 20-month-old fibroblasts stained with TMRM (red) and Hoechst 33342 (blue) following 7c partial chemical reprogramming and *Prkaca* knockdown. Scale bars: 31.1 µm (100 pixels). *C. Effect of 7c partial chemical reprogramming on cellular apoptosis.* 20-month-old fibroblasts were treated with 7c or control vehicle for 1,3, or 6 days followed by staining with DAPI and Annexin V FITC. The percentage of cells undergoing apoptosis (FITC positive,

DAPI negative) was quantified by flow cytometry (n = 3 independent biological replicates). p-values were determined by a two-tailed t-test. ns $p \geq 0.1$, ***$p < 0.001$.

Figure 6 – figure supplement 1: Effect of age on fibroblast metabolome

A. PCA of metabolite samples. PCA was performed following normalization and log-transformation of metabolite peak areas. *B. PCA of untreated fibroblasts.* PCA was performed following normalization and log-transformation of metabolite peak areas. *C. Volcano plots of metabolites affected by partial chemical reprogramming.* Shown in red and blue are metabolites that are significantly elevated and decreased, respectively (FDR < 0.1 and $|\log_2$ fold change$| \geq 1$). Shown in grey are metabolites that are unchanged (FDR ≥ 0.1, or $|\log_2$ fold change$| < 1$).

Figure 7 – figure supplement 1: Expression of pluripotency markers following OSKM reprogramming of fibroblasts

Following doxycycline-induced expression of OSKM in young and old fibroblasts, fully-reprogrammed iPSC colonies were stained for pluripotency markers Sox2 (top), Oct4 (middle), and Nanog (bottom). Representative images obtained from reprogrammed old fibroblasts (left: Hoechst 33342, middle: pluripotency markers, right: merged images). Scale bars: 126.2 µm (100 pixels).

Figure 7 – figure supplement 2: Aging-related changes in the fibroblast epigenome

A. Number of fibroblast CpG sites significantly differentially methylated with age. Shown in cyan and red are sites that experience an increase and decrease in mean methylation with age, respectively. *B. Effect of age on fibroblast mean methylation levels.* p-value was determined by a two-tailed t-test. ns p-value ≥ 0.05. *C. Enrichment analysis of significantly differentially methylated positions (DMPs) that change with fibroblast age for specific chromatin states.* down: DMPs that are hypomethylated with age. up: DMPs that are hypermethylated with age.

Figure 7 – figure supplement 3: Effect of partial chemical reprogramming on the epigenome

A. PCA of DNAm microarray samples. PCA was performed after normalization of array data and filtering of probes. *B. Number of fibroblast CpG sites significantly differentially methylated with 2c and 7c treatment.* Shown in cyan and red are sites that experience an increase and decrease in mean methylation, respectively. *C. Effect of partial chemical reprogramming on fibroblast mean methylation levels.* p-values were determined by one-way ANOVA and Tukey's post-hoc analysis.

ns p-value ≥ 0.05, ***p-value < 0.001. *D. Enrichment analysis of significantly differentially methylated positions (DMPs) that change during partial chemical reprogramming for specific chromatin states.* down: DMPs that are hypomethylated with partial chemical reprogramming. up: DMPs that are hypermethylated with partial chemical reprogramming.

REFERENCES

1 Schumacher, B., Pothof, J., Vijg, J. & Hoeijmakers, J. H. J. The central role of DNA damage in the ageing process. *Nature* **592**, 695-703 (2021). https://doi.org:10.1038/s41586-021-03307-7

2 Hipp, M. S., Kasturi, P. & Hartl, F. U. The proteostasis network and its decline in ageing. *Nature Reviews Molecular Cell Biology* **20**, 421-435 (2019). https://doi.org:10.1038/s41580-019-0101-y

3 Ferrucci, L. & Fabbri, E. Inflammageing: chronic inflammation in ageing, cardiovascular disease, and frailty. *Nature Reviews Cardiology* **15**, 505-522 (2018). https://doi.org:10.1038/s41569-018-0064-2

4 Amorim, J. A. *et al.* Mitochondrial and metabolic dysfunction in ageing and age-related diseases. *Nature Reviews Endocrinology* **18**, 243-258 (2022). https://doi.org:10.1038/s41574-021-00626-7

5 Kane, A. E. & Sinclair, D. A. Epigenetic changes during aging and their reprogramming potential. *Crit Rev Biochem Mol Biol* **54**, 61-83 (2019). https://doi.org:10.1080/10409238.2019.1570075

6 Gems, D. & de Magalhães, J. P. The hoverfly and the wasp: A critique of the hallmarks of aging as a paradigm. *Ageing Res Rev* **70**, 101407 (2021). https://doi.org:10.1016/j.arr.2021.101407

7 Keshavarz, M., Xie, K., Schaaf, K., Bano, D. & Ehninger, D. Targeting the "hallmarks of aging" to slow aging and treat age-related disease: fact or fiction? *Molecular Psychiatry* **28**, 242-255 (2023). https://doi.org:10.1038/s41380-022-01680-x

8 Horvath, S. DNA methylation age of human tissues and cell types. *Genome Biology* **14**, 3156 (2013). https://doi.org:10.1186/gb-2013-14-10-r115

9 Choukrallah, M.-A., Hoeng, J., Peitsch, M. C. & Martin, F. Lung transcriptomic clock predicts premature aging in cigarette smoke-exposed mice. *BMC Genomics* **21**, 291 (2020). https://doi.org:10.1186/s12864-020-6712-z

10 Buckley, M. T. *et al.* Cell-type-specific aging clocks to quantify aging and rejuvenation in neurogenic regions of the brain. *Nature Aging* **3**, 121-137 (2023). https://doi.org:10.1038/s43587-022-00335-4

11 Vaiserman, A. & Krasnienkov, D. Telomere Length as a Marker of Biological Age: State-of-the-Art, Open Issues, and Future Perspectives. *Frontiers in Genetics* **11** (2021). https://doi.org:10.3389/fgene.2020.630186

12 Jansen, R. *et al.* An integrative study of five biological clocks in somatic and mental health. *eLife* **10**, e59479 (2021). https://doi.org:10.7554/eLife.59479

13 Pearce, E. E. *et al.* Telomere length and epigenetic clocks as markers of cellular aging: a comparative study. *Geroscience* **44**, 1861-1869 (2022). https://doi.org:10.1007/s11357-022-00586-4

14 Johnson, A. A., Shokhirev, M. N., Wyss-Coray, T. & Lehallier, B. Systematic review and analysis of human proteomics aging studies unveils a novel proteomic aging clock and identifies key processes that change with age. *Ageing Res Rev* **60**, 101070 (2020). https://doi.org:10.1016/j.arr.2020.101070

15 Krištić, J. *et al.* Glycans are a novel biomarker of chronological and biological ages. *J Gerontol A Biol Sci Med Sci* **69**, 779-789 (2014). https://doi.org:10.1093/gerona/glt190

16 Lu, A. T. *et al.* DNA methylation GrimAge strongly predicts lifespan and healthspan. *Aging (Albany NY)* **11**, 303-327 (2019). https://doi.org:10.18632/aging.101684
17 Sharp, Z. D. & Strong, R. Rapamycin, the only drug that has been consistently demonstrated to increase mammalian longevity. An update. *Experimental Gerontology* **176**, 112166 (2023). https://doi.org:https://doi.org/10.1016/j.exger.2023.112166
18 Shindyapina, A. V. *et al.* Rapamycin treatment during development extends life span and health span of male mice and Daphnia magna. *Science Advances* **8**, eabo5482 (2022). https://doi.org:doi:10.1126/sciadv.abo5482
19 Juricic, P. *et al.* Long-lasting geroprotection from brief rapamycin treatment in early adulthood by persistently increased intestinal autophagy. *Nature Aging* **2**, 824-836 (2022). https://doi.org:10.1038/s43587-022-00278-w
20 Kulkarni, A. S., Gubbi, S. & Barzilai, N. Benefits of Metformin in Attenuating the Hallmarks of Aging. *Cell Metabolism* **32**, 15-30 (2020). https://doi.org:https://doi.org/10.1016/j.cmet.2020.04.001
21 Petkovich, D. A. *et al.* Using DNA Methylation Profiling to Evaluate Biological Age and Longevity Interventions. *Cell Metab* **25**, 954-960.e956 (2017). https://doi.org:10.1016/j.cmet.2017.03.016
22 Zhang, B. *et al.* Multi-omic rejuvenation and lifespan extension upon exposure to youthful circulation. *bioRxiv*, 2021.2011.2011.468258 (2021). https://doi.org:10.1101/2021.11.11.468258
23 Ma, S. *et al.* Heterochronic parabiosis induces stem cell revitalization and systemic rejuvenation across aged tissues. *Cell Stem Cell* **29**, 990-1005.e1010 (2022). https://doi.org:10.1016/j.stem.2022.04.017
24 Yang, J. H. *et al.* Loss of epigenetic information as a cause of mammalian aging. *Cell* **186**, 305-326.e327 (2023). https://doi.org:10.1016/j.cell.2022.12.027
25 Lu, Y. *et al.* Reprogramming to recover youthful epigenetic information and restore vision. *Nature* **588**, 124-129 (2020). https://doi.org:10.1038/s41586-020-2975-4
26 Kriukov, D., Khrameeva, E. E., Gladyshev, V. N., Dmitriev, S. E. & Tyshkovskiy, A. Longevity and rejuvenation effects of cell reprogramming are decoupled from loss of somatic identity. *bioRxiv*, 2022.2012.2012.520058 (2022). https://doi.org:10.1101/2022.12.12.520058
27 Kerepesi, C., Zhang, B., Lee, S. G., Trapp, A. & Gladyshev, V. N. Epigenetic clocks reveal a rejuvenation event during embryogenesis followed by aging. *Sci Adv* **7** (2021). https://doi.org:10.1126/sciadv.abg6082
28 Gladyshev, V. N. The Ground Zero of Organismal Life and Aging. *Trends Mol Med* **27**, 11-19 (2021). https://doi.org:10.1016/j.molmed.2020.08.012
29 Ocampo, A. *et al.* In Vivo Amelioration of Age-Associated Hallmarks by Partial Reprogramming. *Cell* **167**, 1719-1733.e1712 (2016). https://doi.org:10.1016/j.cell.2016.11.052
30 Browder, K. C. *et al.* In vivo partial reprogramming alters age-associated molecular changes during physiological aging in mice. *Nature Aging* **2**, 243-253 (2022). https://doi.org:10.1038/s43587-022-00183-2
31 Guan, J. *et al.* Chemical reprogramming of human somatic cells to pluripotent stem cells. *Nature* **605**, 325-331 (2022). https://doi.org:10.1038/s41586-022-04593-5
32 Hou, P. *et al.* Pluripotent Stem Cells Induced from Mouse Somatic Cells by Small-Molecule Compounds. *Science* **341**, 651-654 (2013). https://doi.org:doi:10.1126/science.1239278
33 Lucas, S. *et al.* Chemical reprogramming ameliorates cellular hallmarks of aging and extends lifespan. *bioRxiv*, 2022.2008.2029.505222 (2022). https://doi.org:10.1101/2022.08.29.505222
34 Au - Khan, M. & Au - Gasser, S. Generating Primary Fibroblast Cultures from Mouse Ear and Tail Tissues. *JoVE*, e53565 (2016). https://doi.org:doi:10.3791/53565

35 Carey, B. W. *et al.* Reprogramming of murine and human somatic cells using a single polycistronic vector. *Proc Natl Acad Sci U S A* **106**, 157-162 (2009). https://doi.org:10.1073/pnas.0811426106
36 Hockemeyer, D. *et al.* A drug-inducible system for direct reprogramming of human somatic cells to pluripotency. *Cell Stem Cell* **3**, 346-353 (2008). https://doi.org:10.1016/j.stem.2008.08.014
37 Schneider, C. A., Rasband, W. S. & Eliceiri, K. W. NIH Image to ImageJ: 25 years of image analysis. *Nature Methods* **9**, 671-675 (2012). https://doi.org:10.1038/nmeth.2089
38 Arneson, A. *et al.* A mammalian methylation array for profiling methylation levels at conserved sequences. *Nature Communications* **13**, 783 (2022). https://doi.org:10.1038/s41467-022-28355-z
39 Zhou, W., Triche, T. J., Jr, Laird, P. W. & Shen, H. SeSAMe: reducing artifactual detection of DNA methylation by Infinium BeadChips in genomic deletions. *Nucleic Acids Research* **46**, e123-e123 (2018). https://doi.org:10.1093/nar/gky691
40 Du, P. *et al.* Comparison of Beta-value and M-value methods for quantifying methylation levels by microarray analysis. *BMC Bioinformatics* **11**, 587 (2010). https://doi.org:10.1186/1471-2105-11-587
41 Vu, H. & Ernst, J. Universal chromatin state annotation of the mouse genome. *Genome Biology* **24**, 153 (2023). https://doi.org:10.1186/s13059-023-02994-x
42 Dobin, A. *et al.* STAR: ultrafast universal RNA-seq aligner. *Bioinformatics* **29**, 15-21 (2013). https://doi.org:10.1093/bioinformatics/bts635
43 Love, M. I., Huber, W. & Anders, S. Moderated estimation of fold change and dispersion for RNA-seq data with DESeq2. *Genome Biology* **15**, 550 (2014). https://doi.org:10.1186/s13059-014-0550-8
44 Robinson, M. D., McCarthy, D. J. & Smyth, G. K. edgeR: a Bioconductor package for differential expression analysis of digital gene expression data. *Bioinformatics* **26**, 139-140 (2009). https://doi.org:10.1093/bioinformatics/btp616
45 Tyshkovskiy, A. *et al.* Identification and Application of Gene Expression Signatures Associated with Lifespan Extension. *Cell Metab* **30**, 573-593.e578 (2019). https://doi.org:10.1016/j.cmet.2019.06.018
46 Tyshkovskiy, A. *et al.* Distinct longevity mechanisms across and within species and their association with aging. *Cell* (2023). https://doi.org:https://doi.org/10.1016/j.cell.2023.05.002
47 Subramanian, A. *et al.* Gene set enrichment analysis: A knowledge-based approach for interpreting genome-wide expression profiles. *Proceedings of the National Academy of Sciences* **102**, 15545-15550 (2005). https://doi.org:doi:10.1073/pnas.0506580102
48 Shen, S. *et al.* rMATS: robust and flexible detection of differential alternative splicing from replicate RNA-Seq data. *Proc Natl Acad Sci U S A* **111**, E5593-5601 (2014). https://doi.org:10.1073/pnas.1419161111
49 Li, J. *et al.* TMTpro-18plex: The Expanded and Complete Set of TMTpro Reagents for Sample Multiplexing. *J Proteome Res* **20**, 2964-2972 (2021). https://doi.org:10.1021/acs.jproteome.1c00168
50 Navarrete-Perea, J., Yu, Q., Gygi, S. P. & Paulo, J. A. Streamlined Tandem Mass Tag (SL-TMT) Protocol: An Efficient Strategy for Quantitative (Phospho)proteome Profiling Using Tandem Mass Tag-Synchronous Precursor Selection-MS3. *J Proteome Res* **17**, 2226-2236 (2018). https://doi.org:10.1021/acs.jproteome.8b00217
51 Rappsilber, J., Ishihama, Y. & Mann, M. Stop and Go Extraction Tips for Matrix-Assisted Laser Desorption/Ionization, Nanoelectrospray, and LC/MS Sample Pretreatment in Proteomics. *Analytical Chemistry* **75**, 663-670 (2003). https://doi.org:10.1021/ac026117i

52 Paulo, J. A. *et al.* Quantitative mass spectrometry-based multiplexing compares the abundance of 5000 S. cerevisiae proteins across 10 carbon sources. *Journal of Proteomics* **148**, 85-93 (2016). https://doi.org:https://doi.org/10.1016/j.jprot.2016.07.005
53 Saba, J., Bonneil, E., Pomiès, C., Eng, K. & Thibault, P. Enhanced Sensitivity in Proteomics Experiments Using FAIMS Coupled with a Hybrid Linear Ion Trap/Orbitrap Mass Spectrometer. *Journal of Proteome Research* **8**, 3355-3366 (2009). https://doi.org:10.1021/pr801106a
54 Chambers, M. C. *et al.* A cross-platform toolkit for mass spectrometry and proteomics. *Nature Biotechnology* **30**, 918-920 (2012). https://doi.org:10.1038/nbt.2377
55 Huttlin, E. L. *et al.* A Tissue-Specific Atlas of Mouse Protein Phosphorylation and Expression. *Cell* **143**, 1174-1189 (2010). https://doi.org:https://doi.org/10.1016/j.cell.2010.12.001
56 Beausoleil, S. A., Villén, J., Gerber, S. A., Rush, J. & Gygi, S. P. A probability-based approach for high-throughput protein phosphorylation analysis and site localization. *Nature Biotechnology* **24**, 1285-1292 (2006). https://doi.org:10.1038/nbt1240
57 Elias, J. E. & Gygi, S. P. Target-decoy search strategy for increased confidence in large-scale protein identifications by mass spectrometry. *Nature Methods* **4**, 207-214 (2007). https://doi.org:10.1038/nmeth1019
58 McAlister, G. C. *et al.* Increasing the Multiplexing Capacity of TMTs Using Reporter Ion Isotopologues with Isobaric Masses. *Analytical Chemistry* **84**, 7469-7478 (2012). https://doi.org:10.1021/ac301572t
59 Goeminne, L. J. E., Gevaert, K. & Clement, L. Experimental design and data-analysis in label-free quantitative LC/MS proteomics: A tutorial with MSqRob. *J Proteomics* **171**, 23-36 (2018). https://doi.org:10.1016/j.jprot.2017.04.004
60 Goeminne, L. J., Gevaert, K. & Clement, L. Peptide-level Robust Ridge Regression Improves Estimation, Sensitivity, and Specificity in Data-dependent Quantitative Label-free Shotgun Proteomics. *Mol Cell Proteomics* **15**, 657-668 (2016). https://doi.org:10.1074/mcp.M115.055897
61 Hornbeck, P. V. *et al.* PhosphoSitePlus, 2014: mutations, PTMs and recalibrations. *Nucleic Acids Research* **43**, D512-D520 (2014). https://doi.org:10.1093/nar/gku1267
62 Divakaruni, A. S., Paradyse, A., Ferrick, D. A., Murphy, A. N. & Jastroch, M. Analysis and interpretation of microplate-based oxygen consumption and pH data. *Methods Enzymol* **547**, 309-354 (2014). https://doi.org:10.1016/b978-0-12-801415-8.00016-3
63 Rojas-Tapias, D. F. *et al.* Inflammation-associated nitrate facilitates ectopic colonization of oral bacterium Veillonella parvula in the intestine. *Nature Microbiology* **7**, 1673-1685 (2022). https://doi.org:10.1038/s41564-022-01224-7
64 Sturm, G. *et al.* Human aging DNA methylation signatures are conserved but accelerated in cultured fibroblasts. *Epigenetics* **14**, 961-976 (2019). https://doi.org:10.1080/15592294.2019.1626651
65 Campbell, P. A. Alkaline Phosphatase Staining. *Bio-protocol* **4**, e1060 (2014). https://doi.org:10.21769/BioProtoc.1060
66 Hagen, T. M. *et al.* Mitochondrial decay in hepatocytes from old rats: Membrane potential declines, heterogeneity and oxidants increase. *Proceedings of the National Academy of Sciences* **94**, 3064-3069 (1997). https://doi.org:doi:10.1073/pnas.94.7.3064
67 Berry, B. J. *et al.* Preservation of mitochondrial membrane potential is necessary for lifespan extension from dietary restriction. *Geroscience* (2023). https://doi.org:10.1007/s11357-023-00766-w
68 Berry, B. J. *et al.* Optogenetic rejuvenation of mitochondrial membrane potential extends C. elegans lifespan. *Nature Aging* **3**, 157-161 (2023). https://doi.org:10.1038/s43587-022-00340-7

69 Shi, G. *et al.* Bend family proteins mark chromatin boundaries and synergistically promote early germ cell differentiation. *Protein Cell* **13**, 721-741 (2022). https://doi.org:10.1007/s13238-021-00884-1
70 Sevilla, A. *et al.* An Esrrb and Nanog Cell Fate Regulatory Module Controlled by Feed Forward Loop Interactions. *Frontiers in Cell and Developmental Biology* **9** (2021). https://doi.org:10.3389/fcell.2021.630067
71 Lowry, W. E. *et al.* Generation of human induced pluripotent stem cells from dermal fibroblasts. *Proceedings of the National Academy of Sciences* **105**, 2883-2888 (2008). https://doi.org:doi:10.1073/pnas.0711983105
72 Takahashi, K. & Yamanaka, S. Induction of pluripotent stem cells from mouse embryonic and adult fibroblast cultures by defined factors. *Cell* **126**, 663-676 (2006). https://doi.org:10.1016/j.cell.2006.07.024
73 Gladyshev, V. N. *et al.* Molecular Damage in Aging. *Nat Aging* **1**, 1096-1106 (2021). https://doi.org:10.1038/s43587-021-00150-3
74 Covelo-Molares, H., Bartosovic, M. & Vanacova, S. RNA methylation in nuclear pre-mRNA processing. *Wiley Interdiscip Rev RNA* **9**, e1489 (2018). https://doi.org:10.1002/wrna.1489
75 Sóti, C. & Csermely, P. Molecular chaperones and the aging process. *Biogerontology* **1**, 225-233 (2000). https://doi.org:10.1023/a:1010082129022
76 Ewald, C. Y. The Matrisome during Aging and Longevity: A Systems-Level Approach toward Defining Matreotypes Promoting Healthy Aging. *Gerontology* **66**, 266-274 (2020). https://doi.org:10.1159/000504295
77 Shpilka, T. & Haynes, C. M. The mitochondrial UPR: mechanisms, physiological functions and implications in ageing. *Nature Reviews Molecular Cell Biology* **19**, 109-120 (2018). https://doi.org:10.1038/nrm.2017.110
78 Turnham, R. E. & Scott, J. D. Protein kinase A catalytic subunit isoform PRKACA; History, function and physiology. *Gene* **577**, 101-108 (2016). https://doi.org:10.1016/j.gene.2015.11.052
79 Zhang, L. *et al.* Role of the Balance of Akt and MAPK Pathways in the Exercise-Regulated Phenotype Switching in Spontaneously Hypertensive Rats. *Int J Mol Sci* **20** (2019). https://doi.org:10.3390/ijms20225690
80 Cheung, H.-H., Liu, X. & Rennert, O. M. Apoptosis: Reprogramming and the Fate of Mature Cells. *ISRN Cell Biology* **2012**, 685852 (2012). https://doi.org:10.5402/2012/685852
81 Paynter, N. P. *et al.* Metabolic Predictors of Incident Coronary Heart Disease in Women. *Circulation* **137**, 841-853 (2018). https://doi.org:10.1161/circulationaha.117.029468
82 Poganik, J. R. *et al.* Biological age is increased by stress and restored upon recovery. *Cell Metabolism* **35**, 807-820.e805 (2023). https://doi.org:https://doi.org/10.1016/j.cmet.2023.03.015
83 Lin, C. C., Chen, Y. P., Yang, W. Z., Shen, J. C. K. & Yuan, H. S. Structural insights into CpG-specific DNA methylation by human DNA methyltransferase 3B. *Nucleic Acids Res* **48**, 3949-3961 (2020). https://doi.org:10.1093/nar/gkaa111
84 Kumar, R., Srivastava, R., Singh, R. K., Surolia, A. & Rao, D. N. Activation and inhibition of DNA methyltransferases by S-adenosyl-L-homocysteine analogues. *Bioorg Med Chem* **16**, 2276-2285 (2008). https://doi.org:10.1016/j.bmc.2007.11.075
85 McBreairty, L. E., Robinson, J. L., Furlong, K. R., Brunton, J. A. & Bertolo, R. F. Guanidinoacetate is more effective than creatine at enhancing tissue creatine stores while consequently limiting methionine availability in Yucatan miniature pigs. *PLoS One* **10**, e0131563 (2015). https://doi.org:10.1371/journal.pone.0131563
86 Wharton, W. & Goz, B. The inhibition by xanthine phosphodiesterase inhibitors of the induction of alkaline phosphatase activity in HeLa cells: Relationship of enzyme activity to cyclic AMP

concentrations. *Journal of Cellular Physiology* **100**, 509-518 (1979). https://doi.org:https://doi.org/10.1002/jcp.1041000313

87 Panyard, D. J., Yu, B. & Snyder, M. P. The metabolomics of human aging: Advances, challenges, and opportunities. *Science Advances* **8**, eadd6155 https://doi.org:10.1126/sciadv.add6155

88 Maffei, M. E. 5-Hydroxytryptophan (5-HTP): Natural Occurrence, Analysis, Biosynthesis, Biotechnology, Physiology and Toxicology. *Int J Mol Sci* **22** (2020). https://doi.org:10.3390/ijms22010181

89 Fukuwatari, T. & Shibata, K. Effect of nicotinamide administration on the tryptophan-nicotinamide pathway in humans. *Int J Vitam Nutr Res* **77**, 255-262 (2007). https://doi.org:10.1024/0300-9831.77.4.255

90 Yamauchi, M. & Sricholpech, M. Lysine post-translational modifications of collagen. *Essays Biochem* **52**, 113-133 (2012). https://doi.org:10.1042/bse0520113

91 Mozhui, K. *et al.* Genetic loci and metabolic states associated with murine epigenetic aging. *eLife* **11**, e75244 (2022). https://doi.org:10.7554/eLife.75244

92 Nishimura, K., Fukuda, A. & Hisatake, K. Mechanisms of the Metabolic Shift during Somatic Cell Reprogramming. *Int J Mol Sci* **20** (2019). https://doi.org:10.3390/ijms20092254

93 Brandt, T. *et al.* Changes of mitochondrial ultrastructure and function during ageing in mice and Drosophila. *eLife* **6**, e24662 (2017). https://doi.org:10.7554/eLife.24662

94 Lu, X. *et al.* Ultrastructural and proteomic profiling of mitochondria-associated endoplasmic reticulum membranes reveal aging signatures in striated muscle. *Cell Death & Disease* **13**, 296 (2022). https://doi.org:10.1038/s41419-022-04746-4

95 Katharine, E. S. *et al.* Age-Related Changes in Axonal and Mitochondrial Ultrastructure and Function in White Matter. *The Journal of Neuroscience* **36**, 9990 (2016). https://doi.org:10.1523/JNEUROSCI.1316-16.2016

96 Warnsmann, V. *et al.* Disruption of the MICOS complex leads to an aberrant cristae structure and an unexpected, pronounced lifespan extension in Podospora anserina. *J Cell Biochem* **123**, 1306-1326 (2022). https://doi.org:10.1002/jcb.30278

97 Zer, V. *et al.* Tri-dimensional Mitochondria Reconstructions of Cardiac Muscle Changes in Size Across Aging due to the MICOS Complex. *bioRxiv*, 2022.2004.2023.489291 (2022). https://doi.org:10.1101/2022.04.23.489291

98 Pellegrini, L. & Scorrano, L. A cut short to death: Parl and Opa1 in the regulation of mitochondrial morphology and apoptosis. *Cell Death & Differentiation* **14**, 1275-1284 (2007). https://doi.org:10.1038/sj.cdd.4402145

99 Sharma, A., Smith, H. J., Yao, P. & Mair, W. B. Causal roles of mitochondrial dynamics in longevity and healthy aging. *EMBO Rep* **20**, e48395 (2019). https://doi.org:10.15252/embr.201948395

100 Rana, A. *et al.* Promoting Drp1-mediated mitochondrial fission in midlife prolongs healthy lifespan of Drosophila melanogaster. *Nature Communications* **8**, 448 (2017). https://doi.org:10.1038/s41467-017-00525-4

101 Semba, R. D., Moaddel, R., Zhang, P., Ramsden, C. E. & Ferrucci, L. Tetra-linoleoyl cardiolipin depletion plays a major role in the pathogenesis of sarcopenia. *Med Hypotheses* **127**, 142-149 (2019). https://doi.org:10.1016/j.mehy.2019.04.015

102 Daum, B., Walter, A., Horst, A., Osiewacz, H. D. & Kühlbrandt, W. Age-dependent dissociation of ATP synthase dimers and loss of inner-membrane cristae in mitochondria. *Proceedings of the National Academy of Sciences* **110**, 15301-15306 (2013). https://doi.org:doi:10.1073/pnas.1305462110

103 Rottenberg, H. & Hoek, J. B. The Mitochondrial Permeability Transition: Nexus of Aging, Disease and Longevity. *Cells* **10** (2021). https://doi.org:10.3390/cells10010079

104 Angeli, S. *et al.* The mitochondrial permeability transition pore activates the mitochondrial unfolded protein response and promotes aging. *eLife* **10**, e63453 (2021). https://doi.org:10.7554/eLife.63453
105 Sun, N., Youle, R. J. & Finkel, T. The Mitochondrial Basis of Aging. *Mol Cell* **61**, 654-666 (2016). https://doi.org:10.1016/j.molcel.2016.01.028
106 Gómez, L. A. & Hagen, T. M. Age-related decline in mitochondrial bioenergetics: does supercomplex destabilization determine lower oxidative capacity and higher superoxide production? *Semin Cell Dev Biol* **23**, 758-767 (2012). https://doi.org:10.1016/j.semcdb.2012.04.002
107 Zhang, H. *et al.* Reduction of elevated proton leak rejuvenates mitochondria in the aged cardiomyocyte. *Elife* **9** (2020). https://doi.org:10.7554/eLife.60827
108 Novack, G. V., Galeano, P., Castaño, E. M. & Morelli, L. Mitochondrial Supercomplexes: Physiological Organization and Dysregulation in Age-Related Neurodegenerative Disorders. *Front Endocrinol (Lausanne)* **11**, 600 (2020). https://doi.org:10.3389/fendo.2020.00600
109 Patron, M. *et al.* Regulation of mitochondrial proteostasis by the proton gradient. *The EMBO Journal* **41**, e110476 (2022). https://doi.org:https://doi.org/10.15252/embj.2021110476
110 Moehle, E. A., Shen, K. & Dillin, A. Mitochondrial proteostasis in the context of cellular and organismal health and aging. *J Biol Chem* **294**, 5396-5407 (2019). https://doi.org:10.1074/jbc.TM117.000893
111 Takahashi, K. & Yamanaka, S. Induction of Pluripotent Stem Cells from Mouse Embryonic and Adult Fibroblast Cultures by Defined Factors. *Cell* **126**, 663-676 (2006). https://doi.org:https://doi.org/10.1016/j.cell.2006.07.024
112 Ohnishi, K. *et al.* Premature Termination of Reprogramming In Vivo Leads to Cancer Development through Altered Epigenetic Regulation. *Cell* **156**, 663-677 (2014). https://doi.org:https://doi.org/10.1016/j.cell.2014.01.005
113 Singh, P. B. & Zhakupova, A. Age reprogramming: cell rejuvenation by partial reprogramming. *Development* **149** (2022). https://doi.org:10.1242/dev.200755
114 Kimmel, J. C. *et al.* Murine single-cell RNA-seq reveals cell-identity- and tissue-specific trajectories of aging. *Genome Res* **29**, 2088-2103 (2019). https://doi.org:10.1101/gr.253880.119
115 Sampathkumar, N. K. *et al.* Widespread sex dimorphism in aging and age-related diseases. *Hum Genet* **139**, 333-356 (2020). https://doi.org:10.1007/s00439-019-02082-w
116 Hothorn, T., Bretz, F. & Westfall, P. Simultaneous inference in general parametric models. *Biom J* **50**, 346-363 (2008). https://doi.org:10.1002/bimj.200810425
117 Xia, J., Psychogios, N., Young, N. & Wishart, D. S. MetaboAnalyst: a web server for metabolomic data analysis and interpretation. *Nucleic Acids Research* **37**, W652-W660 (2009). https://doi.org:10.1093/nar/gkp356

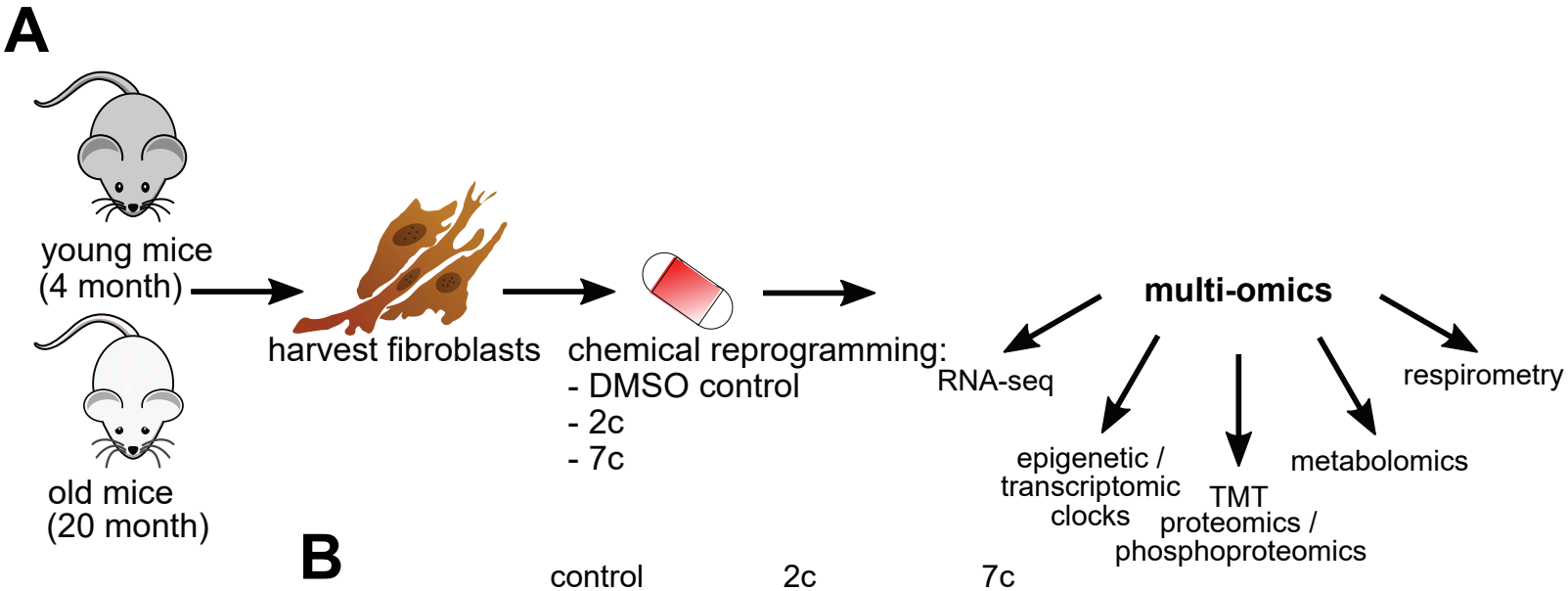
A
young mice
(4 month)
old mice
(20 month)
harvest fibroblasts
chemical reprogramming:
- DMSO control
- 2c
- 7c
multi-omics
RNA-seq
epigenetic /
transcriptomic
clocks
TMT
proteomics /
phosphoproteomics
metabolomics
respirometry

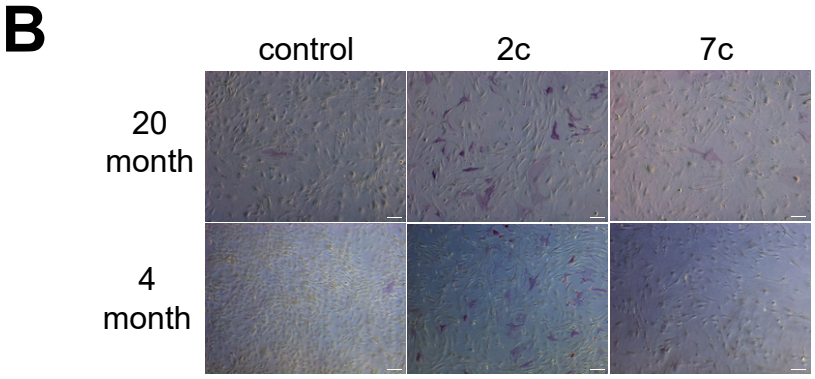
B
control
2c
7c
20
month
4
month

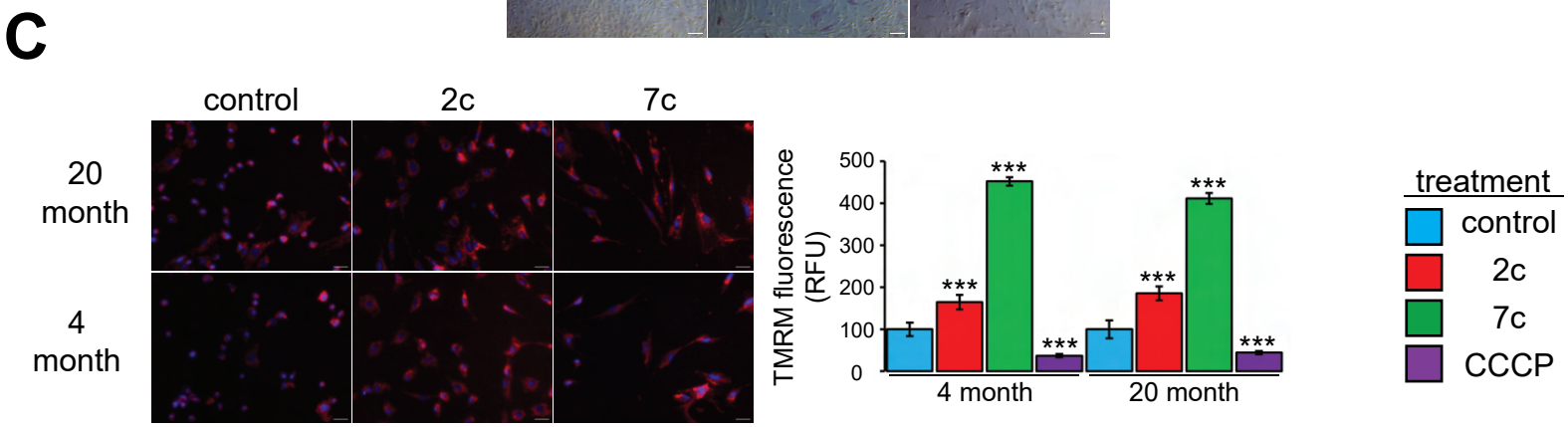
C
control
2c
7c
20
month
4
month
TMRM fluorescence
(RFU)
500
400
300
200
100
0
***
4 month
20 month
treatment
control
2c
7c
CCCP

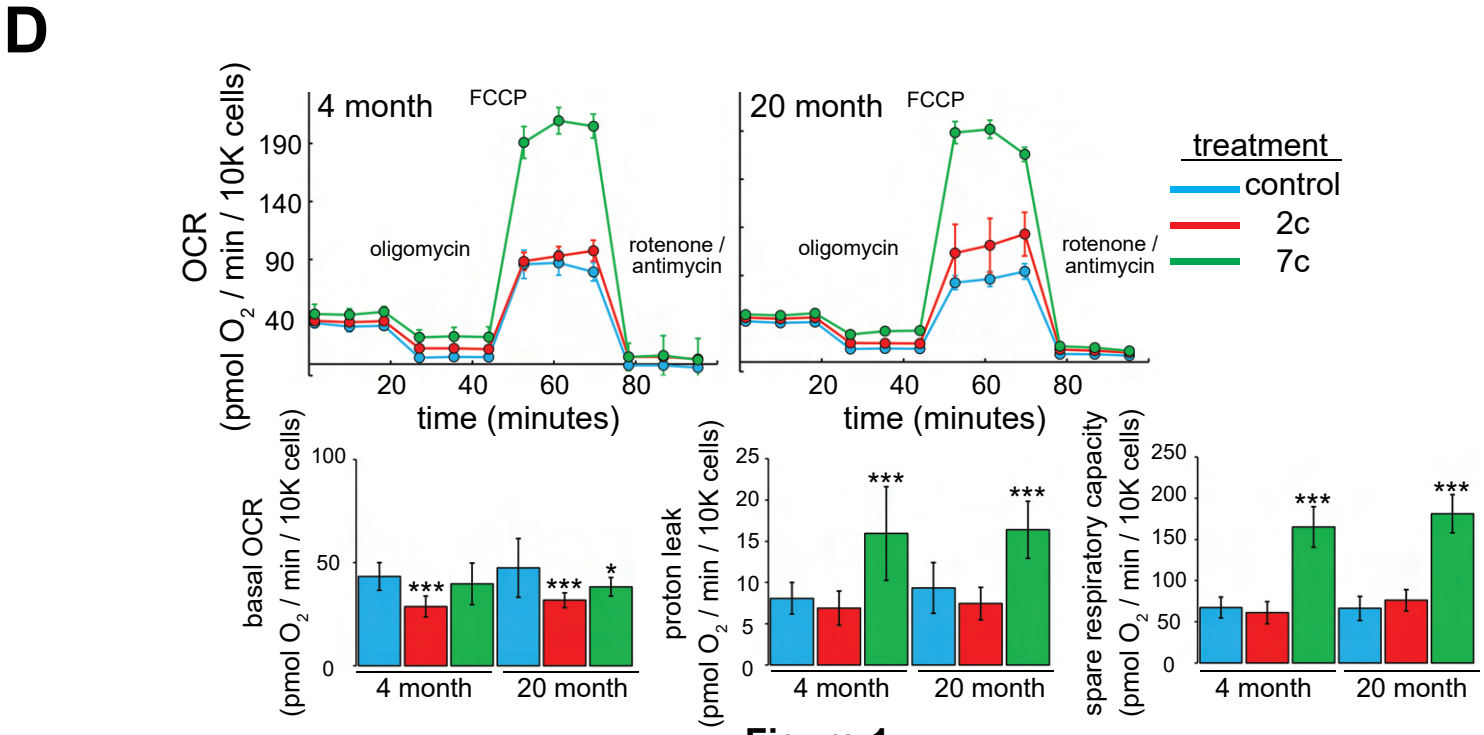
D
4 month
20 month
FCCP
oligomycin
rotenone /
antimycin
OCR
(pmol O2 / min / 10K cells)
190
140
90
40
20
40
60
80
time (minutes)
treatment
control
2c
7c
basal OCR
(pmol O2 / min / 10K cells)
100
50
0
proton leak
(pmol O2 / min / 10K cells)
25
20
15
10
5
spare respiratory capacity
(pmol O2 / min / 10K cells)
250
200
150
100
50
***
*
4 month
20 month

Figure 1

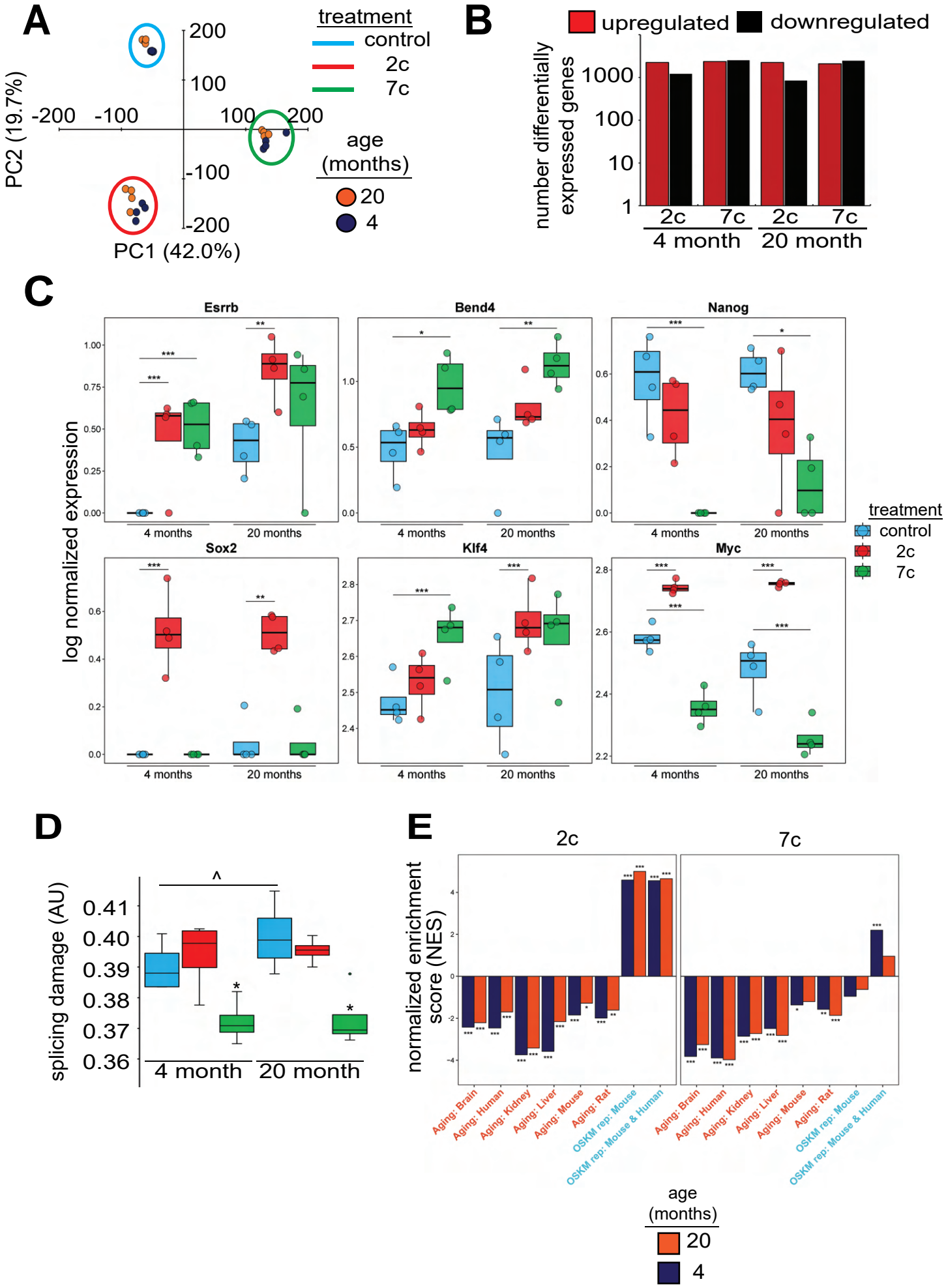
A
treatment
control
2c
7c
age (months)
20
4
PC2 (19.7%)
PC1 (42.0%)
B
upregulated
downregulated
number differentially expressed genes
2c
7c
4 month
20 month
C
Esrrb
Bend4
Nanog
Sox2
Klf4
Myc
log normalized expression
4 months
20 months
treatment
control
2c
7c
D
splicing damage (AU)
4 month
20 month
E
2c
7c
normalized enrichment score (NES)
Aging: Brain
Aging: Human
Aging: Kidney
Aging: Liver
Aging: Mouse
Aging: Rat
OSKM rep: Mouse
OSKM rep: Mouse & Human
age (months)
20
4

Figure 2

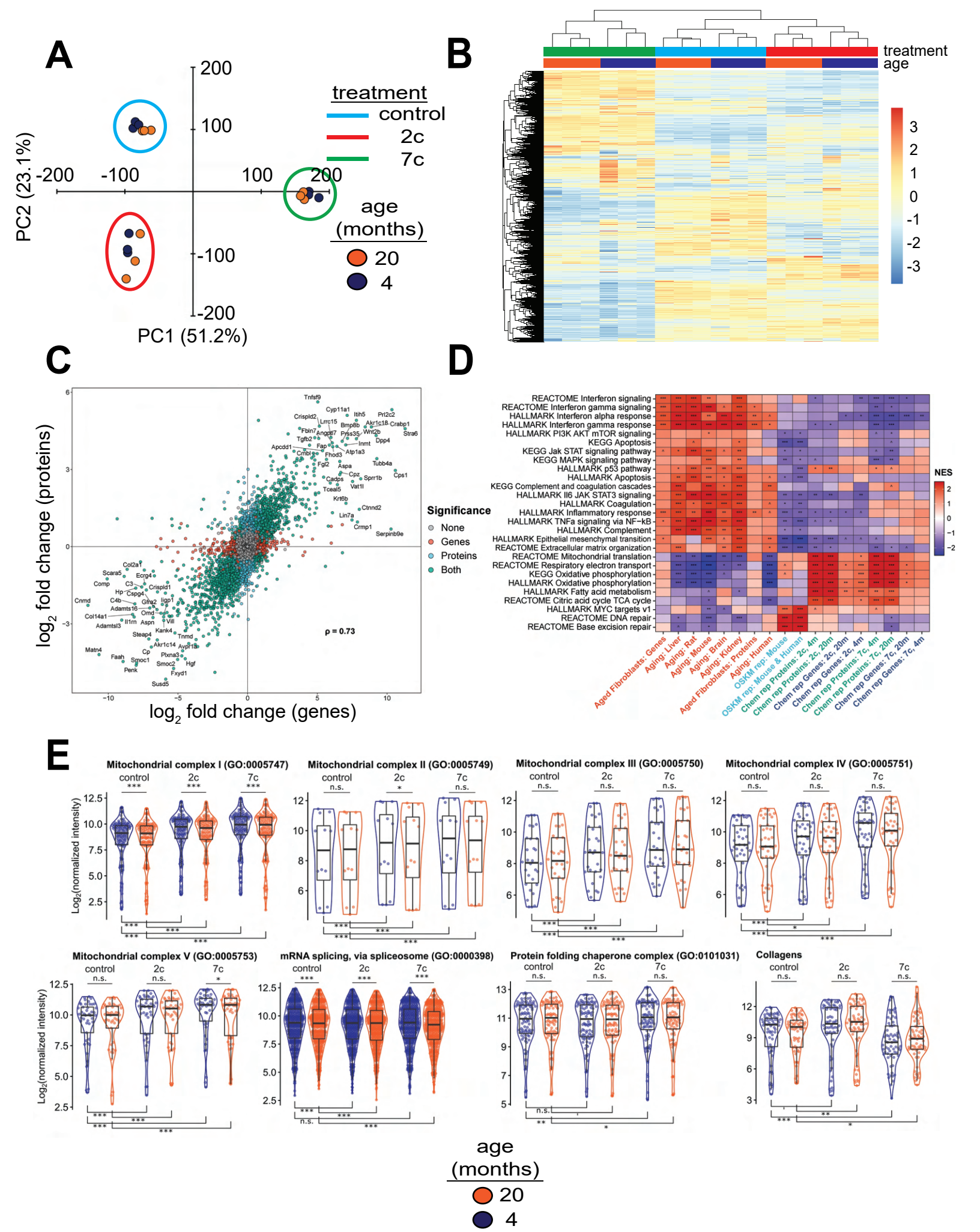
A
PC2 (23.1%)
PC1 (51.2%)
treatment
control
2c
7c
age (months)
20
4
B
treatment
age
C
log2 fold change (proteins)
log2 fold change (genes)
ρ = 0.73
Significance
None
Genes
Proteins
Both
D
NES
REACTOME Interferon signaling
REACTOME Interferon gamma signaling
HALLMARK Interferon alpha response
HALLMARK Interferon gamma response
HALLMARK PI3K AKT mTOR signaling
KEGG Apoptosis
KEGG Jak STAT signaling pathway
KEGG MAPK signaling pathway
HALLMARK p53 pathway
HALLMARK Apoptosis
KEGG Complement and coagulation cascades
HALLMARK Il6 JAK STAT3 signaling
HALLMARK Coagulation
HALLMARK Inflammatory response
HALLMARK TNFa signaling via NF-kB
HALLMARK Complement
HALLMARK Epithelial mesenchymal transition
REACTOME Extracellular matrix organization
REACTOME Mitochondrial translation
REACTOME Respiratory electron transport
KEGG Oxidative phosphorylation
HALLMARK Oxidative phosphorylation
HALLMARK Fatty acid metabolism
REACTOME Citric acid cycle TCA cycle
HALLMARK MYC targets v1
REACTOME DNA repair
REACTOME Base excision repair
Aged Fibroblasts: Genes
Aging: Liver
Aging: Rat
Aging: Mouse
Aging: Brain
Aging: Kidney
Aged Fibroblasts: Proteins
Aging: Human
OSKM rep: Mouse
OSKM rep: Mouse & Human
Chem rep Proteins: 2c, 4m
Chem rep Proteins: 2c, 20m
Chem rep Genes: 2c, 20m
Chem rep Genes: 2c, 4m
Chem rep Proteins: 7c, 4m
Chem rep Proteins: 7c, 20m
Chem rep Genes: 7c, 20m
Chem rep Genes: 7c, 4m
E
Mitochondrial complex I (GO:0005747)
Mitochondrial complex II (GO:0005749)
Mitochondrial complex III (GO:0005750)
Mitochondrial complex IV (GO:0005751)
Mitochondrial complex V (GO:0005753)
mRNA splicing, via spliceosome (GO:0000398)
Protein folding chaperone complex (GO:0101031)
Collagens
control
2c
7c
Log2(normalized intensity)
age (months)
20
4

Figure 3

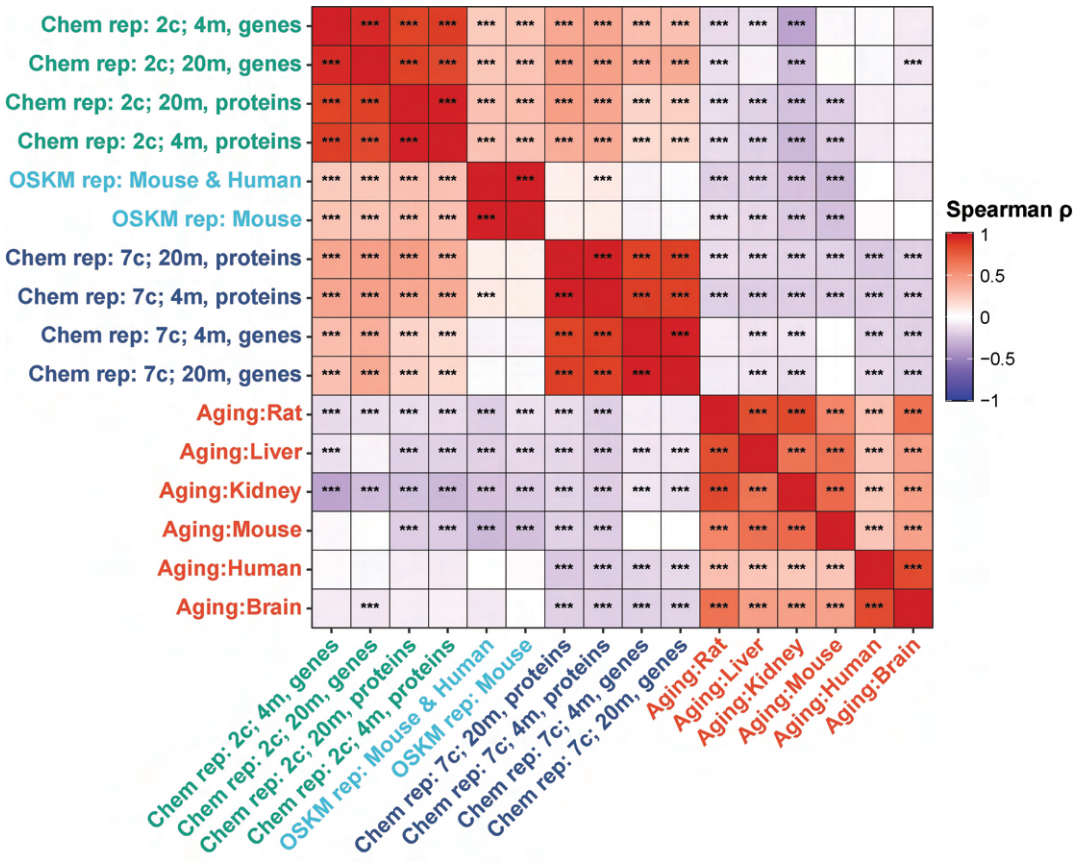
Chem rep: 2c; 4m, genes
Chem rep: 2c; 20m, genes
Chem rep: 2c; 20m, proteins
Chem rep: 2c; 4m, proteins
OSKM rep: Mouse & Human
OSKM rep: Mouse
Chem rep: 7c; 20m, proteins
Chem rep: 7c; 4m, proteins
Chem rep: 7c; 4m, genes
Chem rep: 7c; 20m, genes
Aging:Rat
Aging:Liver
Aging:Kidney
Aging:Mouse
Aging:Human
Aging:Brain
Spearman ρ
1
0.5
0
−0.5
−1

Figure 4

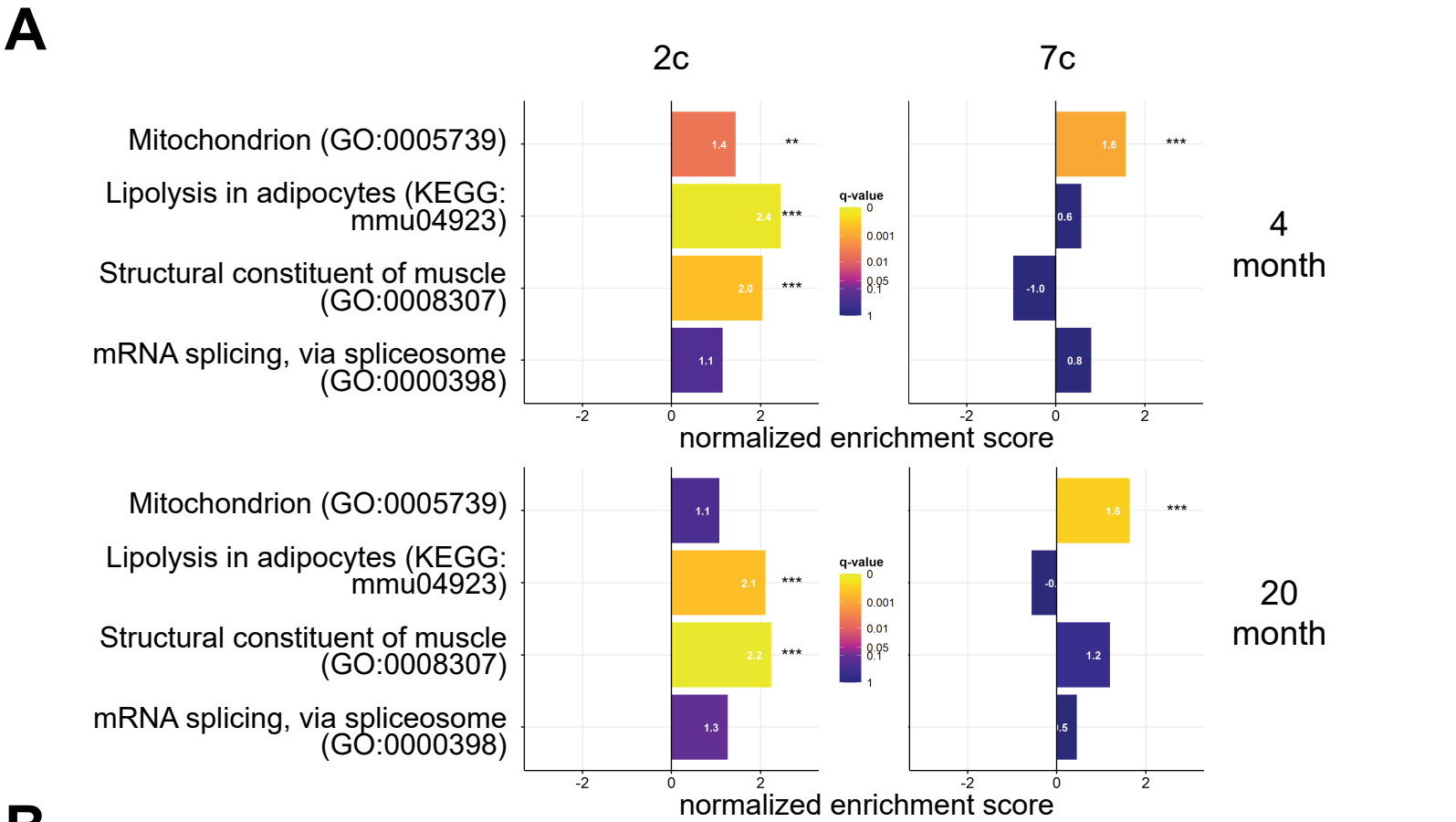
A
2c
7c
Mitochondrion (GO:0005739)
Lipolysis in adipocytes (KEGG: mmu04923)
Structural constituent of muscle (GO:0008307)
mRNA splicing, via spliceosome (GO:0000398)
q-value
4 month
20 month
normalized enrichment score

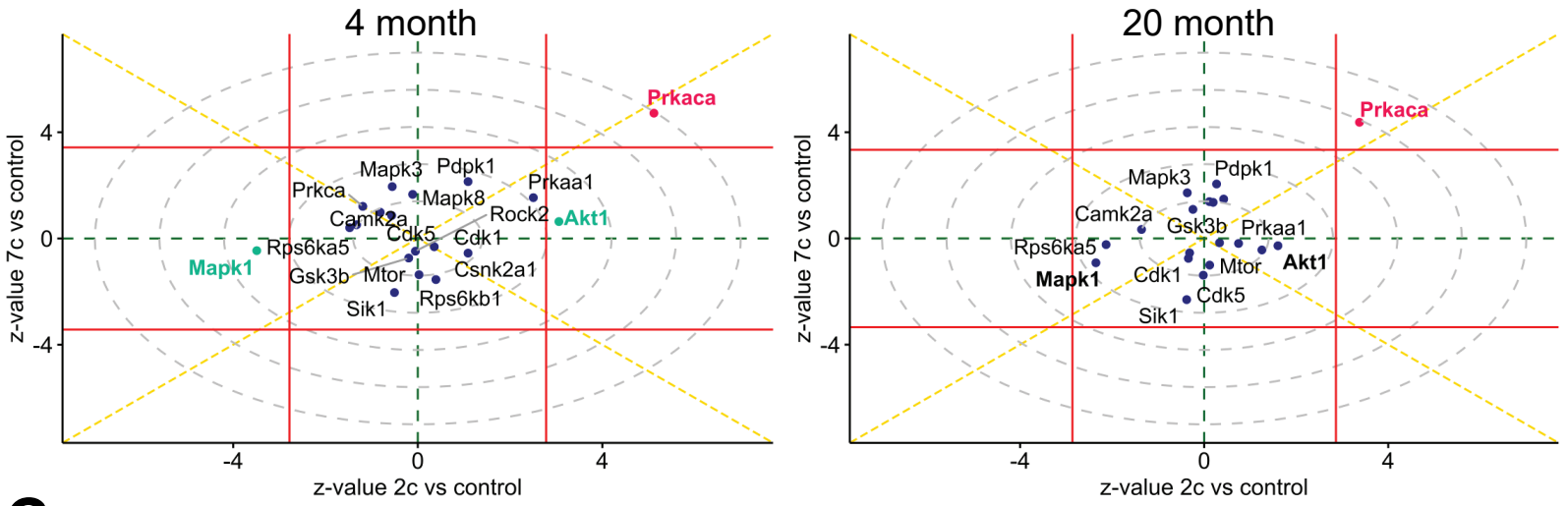
B
4 month
20 month
Prkaca
Mapk3
Pdpk1
Prkca
Mapk8
Prkaa1
Camk2a
Rock2
Akt1
Cdk5
Cdk1
Rps6ka5
Mapk1
Gsk3b
Mtor
Csnk2a1
Sik1
Rps6kb1
z-value 7c vs control
z-value 2c vs control

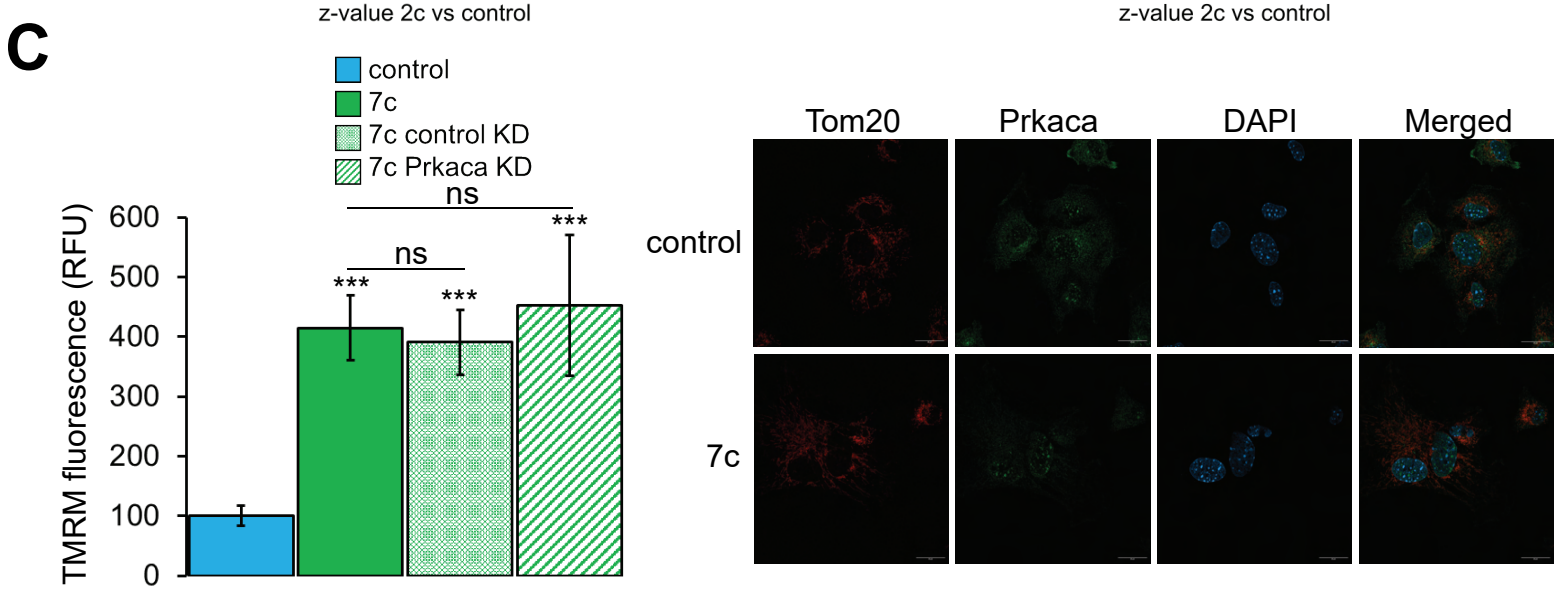
C
control
7c
7c control KD
7c Prkaca KD
ns
TMRM fluorescence (RFU)
Tom20
Prkaca
DAPI
Merged

Figure 5

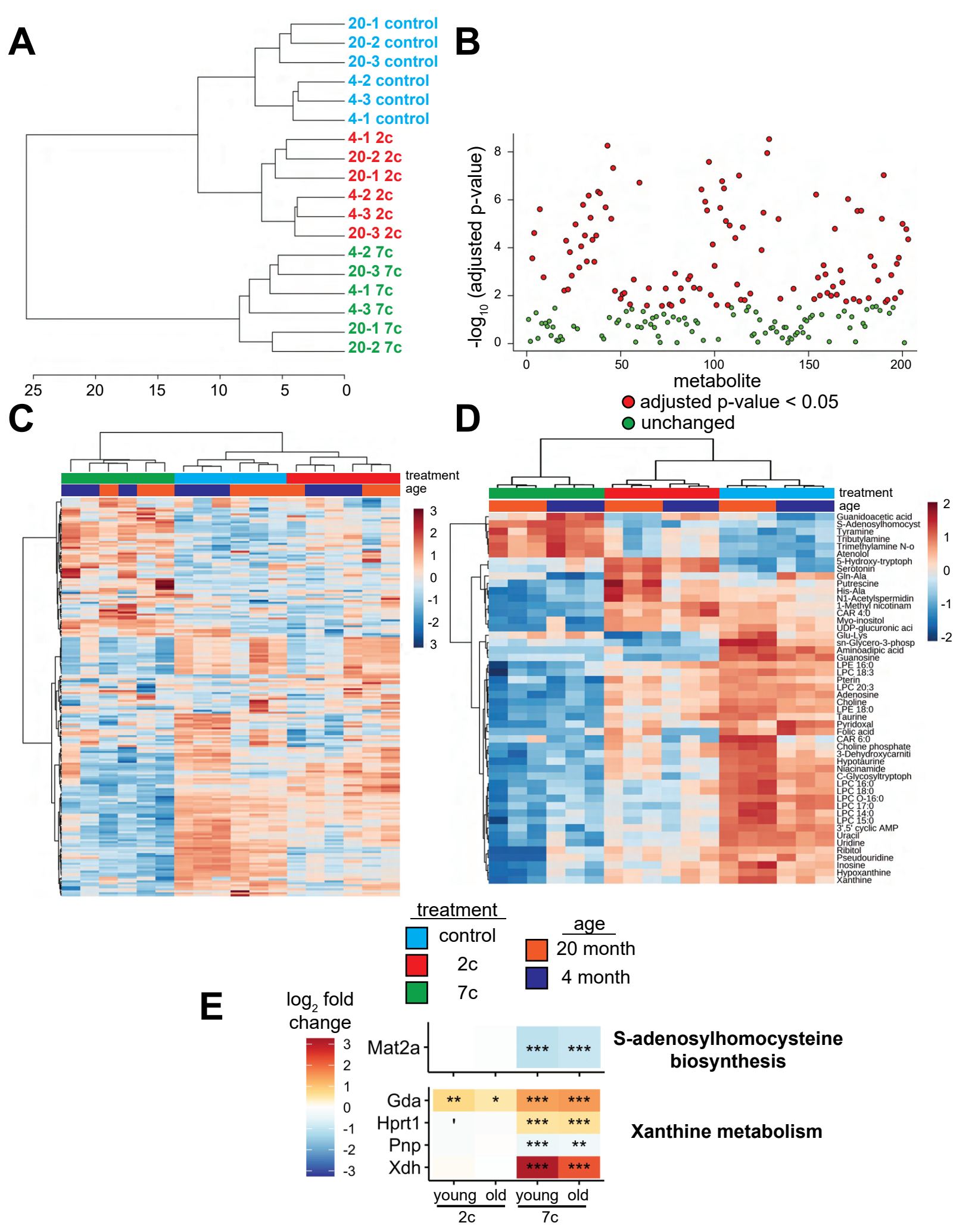
A
20-1 control
20-2 control
20-3 control
4-2 control
4-3 control
4-1 control
4-1 2c
20-2 2c
20-1 2c
4-2 2c
4-3 2c
20-3 2c
4-2 7c
20-3 7c
4-1 7c
4-3 7c
20-1 7c
20-2 7c
25 20 15 10 5 0
B
-log10 (adjusted p-value)
metabolite
adjusted p-value < 0.05
unchanged
C
treatment
age
D
treatment
age
Guanidoacetic acid
S-Adenosylhomocyst
Tyramine
Tributylamine
Trimethylamine N-o
Atenolol
5-Hydroxy-tryptoph
Serotonin
Gln-Ala
Putrescine
His-Ala
N1-Acetylspermidin
1-Methyl nicotinam
CAR 4:0
Myo-inositol
UDP-glucuronic aci
Glu-Lys
sn-Glycero-3-phosp
Aminoadipic acid
Guanosine
LPE 16:0
LPC 18:3
Pterin
LPC 20:3
Adenosine
Choline
LPE 18:0
Taurine
Pyridoxal
Folic acid
CAR 6:0
Choline phosphate
3-Dehydroxycarniti
Hypotaurine
Niacinamide
C-Glycosyltryptoph
LPC 16:0
LPC 18:0
LPC O-16:0
LPC 17:0
LPC 14:0
LPC 15:0
3',5' cyclic AMP
Uracil
Uridine
Ribitol
Pseudouridine
Inosine
Hypoxanthine
Xanthine
treatment
control
2c
7c
age
20 month
4 month
E
log2 fold change
Mat2a
S-adenosylhomocysteine biosynthesis
Gda
Hprt1
Pnp
Xdh
Xanthine metabolism
young old young old
2c 7c

Figure 6

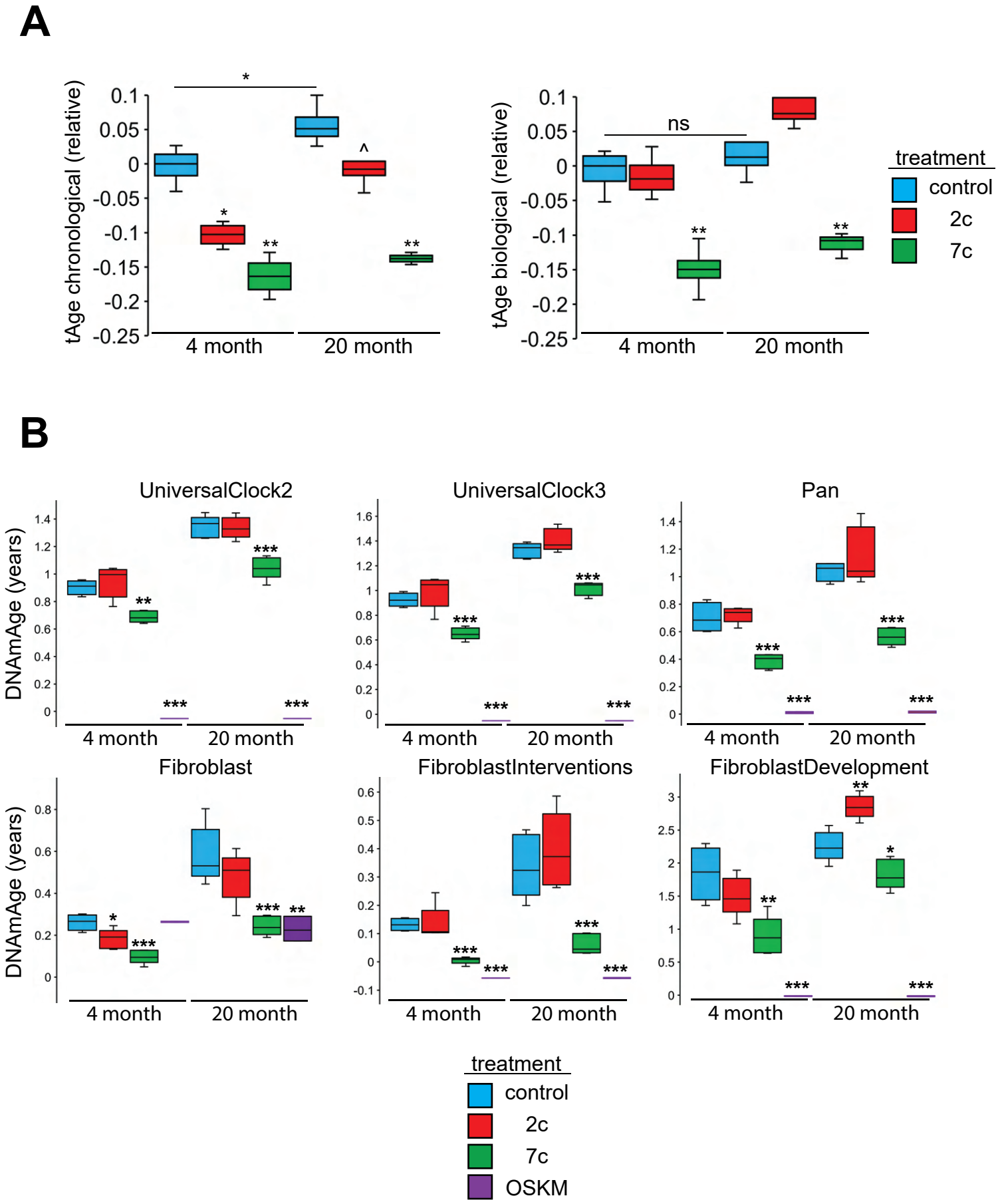
A
tAge chronological (relative)
tAge biological (relative)
4 month
20 month
ns
treatment
control
2c
7c
B
UniversalClock2
UniversalClock3
Pan
Fibroblast
FibroblastInterventions
FibroblastDevelopment
DNAmAge (years)
OSKM

Figure 7